UTRECHT UNIVERSITY

MSc THESIS

Dispersivity-Saturation relationship for various porous media; Experiments and modelling

Author:
Riemer DE WITTE

Supervisor:
dr. Mojtaba G. MAHMOODLU
dr. Amir RAOOF

A Thesis submitted in fulfillment of the requirements for the degree of MSc Hydrology

in the

Environmental Hydrogeology Research Group
Department of Earth Sciences

March 1, 2017

Utrecht University

Abstract

Faculty of Geosciences
Department of Earth Sciences

MSc Hydrology

Dispersivity-Saturation relationship for various porous media; Experiments and modelling

by Riemer DE WITTE

Dispersion of solutes has been studied widely in saturated porous media. However, unsaturated porous media lacks substantial experimental data to provide correlation on the saturation-dependency of hydrodynamic dispersion. This study aims to provide experimental data through $CaCl_2$ injections in unit hydraulic gradient unsaturated sandy porous media at lab-scale columns (z = 37 cm). Dispersivity (α) as a function of wetting phase saturation (S_w) are extracted from measured electrical conductivity at equidistant depths along the column. Results show a clear non-monotonic $\alpha - S_w$ relation, with a maximum dispersivity of 1.32 cm at a saturation (S_w) of 0.43 [-] for a porous medium with D_{50} of 500 μm. For both S_w <0.39 and S_w >0.43, α decreases. For higher saturations, α decreases until a saturated α of 0.05 cm. For lower saturation, α decreases until only diffusion is the dominant process of solute displacement. Tailing is observed in all unsaturated experiments, indicating stagnant zones in the flow domain. Comparison with literature shows a resemblance for dispersivity values corresponding to S_w >0.43. For S_w <0.43, experimental results by this study confirm numerical porenetwork results by Raoof and Hassanizadeh (2013) and experimental results by Toride et al. (2003). The accuracy of dispersivity over the entire range of saturation resulted in a general equation describing the phenomenon. Dispersivity is calculated as a function of wetting phase saturation for a specific set of constants a,b, and c by $\alpha = ae^{(-(\frac{S_w - b}{c})^2)}$. An approach for scaling the results of this study through intrinsic soil parameters is proposed. Hopefully, results from this study help improve accuracy of contaminant, virus, and colloids fate and transport in the unsaturated zone.

Contents

Abstract **i**

1 Introduction **1**
1.1 Unsaturated transport principles 1
1.2 Literature on experimental unsaturated dispersivity 2
1.3 Objective 2

2 Experimental setup & Materials **4**
2.1 Experimental setup 4
2.2 Materials & measuring equipment 5
2.2.1 Column 5
2.2.2 Tensiometer 5
2.2.3 5TE-sensor 6
2.3 Porous media characteristics 6

3 Methods **8**
3.1 Saturated flow experiment 8
3.2 Unsaturated flow experiment 9
3.3 Column preparation 10
3.4 Retention data 11
3.5 Conductivity measurements 12
3.6 Data analysis 12
3.6.1 Advection-Dispersion model 12
3.6.2 Mobile-Immobile model 13

4 Results **14**
4.1 Unsaturated hydraulic conductivity 14
4.2 Analysis of experimental data 14
4.2.1 Modelling by Advection-Dispersion model 14
4.2.2 Modelling by Mobile-Immobile model 17
4.3 Analysis of saturation dependency 19
4.4 Analysis of scale-effect 24
4.5 Retention data 24

5 Discussion **26**

6 Conclusion **28**

A Calibration data **29**

B Concentration effect on permittivity **30**

C Dispersivity-Saturation relation at three different depths **31**

D Dispersivity-Saturation relation compared to literature **32**

E 5TE Specifications **33**

List of Figures

2.1 Schematic of experimental setup, numbers indicating various components . . 4
2.2 Tensiometer used for soil moisture pressure measurements inside the column 5
2.3 The 5TE-sensor used in the experiment, figure from Decagon Devices (2016). 6
2.4 Grain size distribution of S1 7

3.1 Schematic illustration of the constant head method 8
3.2 Schematic illustration of the starting condition (saturated; left), and the initial condition for the unsaturated solute displacement experiment (unsaturated; right). The position of the constant matric potential profile varies with saturation of the porous medium. A lower saturation will shift the matric potential to the left, whereas a higher saturation will move ψ to the right. 10
3.3 Schematic figure of the HYPROP device for measuring retention data. Figure reproduced with permission from Schindler et al. (2010) 11

4.1 Hydraulic conductivity as a function of saturation for S1 14
4.2 Breakthrough curves under saturated condition (S_w=1) at three locations (11.5, 19 and 26.5 cm) from inlet. Flux = 0.341 cm min^{-1}. Points indicate data, lines indicate fit by ADE-model in CXTFIT 15
4.3 Breakthrough curves under unsaturated condition (S_w=0.5) at three locations (10.5, 18 and 25.5 cm) from inlet. Flux = 0.420 cm min^{-1}. Matric potential = -16.7$\pm$0.5 cm. Points indicate data, lines indicate fit by ADE-model in CXTFIT 16
4.4 Breakthrough curves under unsaturated condition (S_w=0.25) at three locations (10.5, 18 and 25.5 cm) from inlet. Flux = 0.010 cm min^{-1}. Matric potential = -23.35$\pm$0.3 cm. Points indicate data, lines indicate fit by ADE-model in CXTFIT 16
4.5 Schematic pressure diagram showing the position of furthest 5TE sensor from inlet. non-unit gradient conditions below the sensor influence the dispersion coefficient. 17
4.6 Shows the Mobile dispersivity (α_m) as a function of saturation, the data is from the middle of column (z = 18 cm) 18
4.7 Shows the Mobile water content fraction (β) as a function of saturation, the data is from the middle of column (z = 18 cm) 19
4.8 Dispersivity distribution as a function of saturation, data points indicating dispersivity for a certain saturation for depths of 10.5, 18, and 25 cm 21
4.9 Pore space distribution under varying conditions. top: (near-) residual saturation; middle: intermediate saturation; bottom: saturated. 22
4.10 Representation of porous medium, slightly exaggerated differences between pore radii to illustrate hydrodynamic dispersion under unsaturated conditions. Left: mesopore flow; middle: macropore flow; right: micropore flow. . 23
4.11 Scale effect of the dispersion coefficient 24
4.12 Retention curve of S1, fitted with the van Genuchten equation (van Genuchten, 1980). 25

4.13 Retention curve of S3, fitted with the van Genuchten equation (van Genuchten, 1980). 25

A.1 Showing three graphs, each one representing the calibration curve for measured EC_b versus concentration. Top figure: 5TE-1, Middle figure: 5TE-2, bottom figure: 5TE-3. 29

B.1 Showing EC_p values as calculated with the equation developed by Hilhorst (Eq. 3.7) 30

C.1 Showing the α - S_w relation for all three depths, including a separately fitted Gaussian function 31

D.1 Showing the α - S_w relation for the results from this study, the model values using Equation 4.3, the experimental results by Toride et al. (2003), Padilla et al. (1999) and pore-scale results by Raoof and Hassanizadeh (2013) 32

E.1 Shows specifications of the 5TE sensor used for measuring permittivity, electrical conductivity and temperature, from Decagon Devices (2016) 33

List of Tables

2.1 Porous media characteristics 7

3.1 Advection-Dispersion & Mobile-Immobile conditions 13

4.1 Experimental data from saturated flow experiments for three porous media, all values are from the middle section of the column (z = 18 cm) 15
4.2 MIM-model results 19
4.3 Experimental data from unsaturated flow experiments for porous medium S1, at depth z = 18 cm (5TE-2) 20

List of Abbreviations

5TE-1	Electrical conductivity sensor 1 (z=10.5 cm)
5TE-2	Electrical conductivity sensor 2 (z=18.0 cm)
5TE-3	Electrical conductivity sensor 3 (z=25.5 cm)
S1	Sand 1, porous medium with D_{50} 500 μm
S2	Sand 2, porous medium with D_{50} 215 μm
S3	Sand 3, porous medium with D_{50} 130 μm
CXTFIT	Modelling software for analyzing breakthrough curves

List of Symbols

Symbol	*description*	*unit*
α	dispersivity	L
α^*	Van Genuchten parameter	-
β	Mobile fraction of water content	-
θ	volumetric water content	$L^3\ L^{-3}$
θ_m	Mobile water content	$L^3\ L^{-3}$
θ_{im}	Immobile volumetric water content	$L^3\ L^{-3}$
θ_s	Saturated volumetric water content	$L^3\ L^{-3}$
θ_r	Residual volumetric water content	$L^3\ L^{-3}$
θ_s	Saturated volumetric water content	$L^3\ L^{-3}$
ϕ	Porosity	$L^3\ L^{-3}$
Φ	Sorting coefficient	-
ψ	pressure head (matric potential)	L
ω	Mass transfer coefficient	T^{-1}
a	constant in dispersivity estimation equation	-
A	Area	L^2
A_0	Calibration constant for 5TE-sensor	-
b	constant in dispersivity estimation equation	-
B_0	Calibration constant for 5TE-sensor	-
c_0	constant in dispersivity estimation equation	-
c	concentration	$M\ L^{-3}$
c_m	Concentration of solutes in mobile fraction of water content	$M\ L^{-3}$
c_{im}	Concentration of solutes in immobile fraction of water content	$M\ L^{-3}$
C_0	Concentration at time = 0	$M\ L^{-3}$
C_1	Concentration at ime = 1	$M\ L^{-3}$
C_n	Normalized concentration to maximum concentration	-
d	Particle diameter size	L
D	Dispersion coefficient	$L^2\ T^{-1}$
D_e	Effective diffusion coefficient	$L^2\ T^{-1}$
EC_b	Bulk electrical conductivity	$\mu S\ L^{-1}$
EC_p	Pore electrical conductivity	$\mu S\ L^{-1}$
E_b	dielectric constant of bulk soil	-
E_p	dielectric constant of soil pore water	-
E_{b0}	dielectric constant of the sand	-
h	pressure head (matric potential)	L
H	Total hydraulic head	L
K	Hydraulic conductivity	$L\ T^{-1}$
m	Van Genuchten parameter	-
n	Van Genuchten parameter	-
P_e	Peclet number	-
q	darcy flux	$L\ T^{-1}$
R	Retardation factor	-

S_w	Saturation	-
t	time	T
v	pore-water velocity	$L^2\ T^{-1}$
V	Volume	L^3
z	elevation head	L

1 Introduction

1.1 Unsaturated transport principles

Dispersion of a solute is the deviation of a solute from the mean displacement as a function of irregularities in the flow paths of the fluid. For a homogeneous soil and conservative solute, the hydrodynamic dispersion in one dimension is accurately described in the advection-dispersion equation (ADE), (Bear, 1972).

$$D\frac{\partial^2 c}{\partial z^2} - v\frac{\partial c}{\partial z} = R\frac{\partial c}{\partial t} \tag{1.1}$$

Where D is the hydrodynamic dispersion coefficient [$L^2\ T^{-1}$], c the solute concentration [M L^{-3}], z the (downward) direction of flow [L], v the pore-water flow velocity [L T^{-1}], R the retardation factor [-], and t is time [T]. The first term describes the concentration change by hydrodynamic dispersion as a deviation from the second term, the advective term. Both are calculated as a function of change over time and volumetric water content.

The degree of dispersion is a function of average flow velocity and saturation of the porous medium. The previous is linearly related for saturated porous media, as proven by Bear (1972).

$$D(v) = D_e + \alpha v \tag{1.2}$$

Where D is the dispersion coefficient [$L^2\ T^{-1}$], D_e the effective diffusion coefficient [$L^2\ T^{-1}$], α the dispersivity $[L]$ and v the velocity [$L\ T^{-1}$].

However, to account for the volumetric water content of the porous medium, the dispersion coefficient must be written as a function of both water content and velocity.

$$D(v,\theta) = D_e(\theta) + \alpha(\theta)v \tag{1.3}$$

Diffusion is described as a fickian process of random motion where solutes follow a gradient from high to low concentration, and is quantified by the tortuosity based model for estimation of the effective diffusivity in unsaturated porous media (Eq. 1.4) (Millington and Quirk, 1961).

$$D_e(\theta) = D_0\frac{\theta^{10/3}}{\phi^2} \tag{1.4}$$

Where D_0 is the aqueous diffusion coefficient [$L^2\ T^{-1}$], ϕ is the porosity of the porous medium [-], and θ is the volumetric water content [-]. The contribution of molecular diffusion to the total dispersion coefficient is usually negligible for most flow velocities. However, it can become important at lower flow velocity conditions, as is evident from Equation 1.5. The relative effect of advection to molecular diffusion is typically quantified by the Peclet number. Since the mechanical dispersion is linearly related to advection, this is also the relative degree of influence of mechanical dispersion over molecular diffusion. The following expression quantifies this relative contribution, first presented in this form by Freeze

and Cherry (1979):

$$P_e = \frac{vd}{D_e} \tag{1.5}$$

Where v is the velocity of the fluid [L T^{-1}], d is a characteristic length [L], i.e. the mean soil particle radius, and D_e is the effective molecular diffusion coefficient [L^2 T^{-1}].

1.2 Literature on experimental unsaturated dispersivity

The relation between saturation of the porous medium and hydrodynamic dispersion has not been properly validated to date, e.g. the effect of the saturation (S_w) on the dispersivity (α) in Equation 1.3 is not established to an extent that is sufficient to describe in a mathematic sense. Various studies indicates different relationships between the saturation of a porous medium and dispersivity (Toride et al., 2003; Maraqa et al., 1997; Padilla et al., 1999; Kanzari et al., 2015; Maciejewski, 1993). Maciejewski (1993) showed that the dispersivity increases linearly with decreasing saturation, Kanzari et al. (2015) indicate an increasing dispersivity with decreasing saturation, which can be described by a low power function. Whereas results by Toride et al. (2003) show a likewise trend. However, for that study, the dispersivity also decreases after a certain intermediate saturation.

Literature on unsaturated hydrodynamic dispersion have shown a significant change in the symmetry of the breakthrough curve when desaturating the porous medium (Gupta et al., 1973; Krupp and Elrick, 1968; Toride et al., 2003; Maraqa et al., 1997; Kanzari et al., 2015; Nützmann et al., 1998). This effect is labeled tailing and indicates that there are larger heterogeneities in the flow field of the fluid as opposed to flow in saturated media, as well as presence of immobile water (e.g. (De Smedt and Wierenga, 1984; Gupta et al., 1973)). Tailing causes the shape of the breakthrough curve to change in the rising limb at the top, i.e. flattening, while at the falling limb it extends the length of the breakthrough curve. These changes during unsaturated flow indicate a higher hydrodynamic dispersion, first recognized with a glass bead experiment by De Smedt and Wierenga (1984).

1.3 Objective

The main goal of this study is to quantify saturation dependent solute dispersivity. The following steps are carried out in order to understand the characteristics of the sand, and interpret the flow of fluids and solutes through the porous medium.

An experimental sand column with a length of 37 cm and diameter of 9.5 cm is prepared to measure dispersivity as a function of saturation. The range of saturation is from 0.25 [-] to 1 [-] (saturated). Bulk electrical conductivity (EC_b) is monitored at three equidistant depths (z = 10.5, 18, and 25.5 cm) along the column. These measurements are fitted using the analytical model CXTFIT (Toride et al., 1995), solving for the ADE model as well as the Mobile-Immobile (MIM) model. In order to validate the conclusion of the experiment, the data will be compared to the existing literature on unsaturated dispersivity by previously mentioned authors (Toride et al., 2003; Maraqa et al., 1997; Padilla et al., 1999; Kanzari et al., 2015; Maciejewski, 1993) as well as compared to a numerical pore scale model by Raoof and Hassanizadeh (2013).

By being able to mathematically express the relation of α with S_w, this study aims to provide a solid foundation for unsaturated zone modelling. Dispersion of fluids can be considered as a key factor influencing transport of viruses, colloids, and dissolved contaminants, therefore, the results of this study hopes to enable the scientific community to assess a realistic scenario of residence times and storage of contaminants in the unsaturated zone.

2 Experimental setup & Materials

2.1 Experimental setup

Figure 2.1 shows a schematic of the experimental setup. On top of the figure are two 10-liter glass laboratory bottles [no. 1a & 1b]. These bottles are reservoirs for the degassed DI-water and $CaCl_2$-solution feed. Both influent solution bottles are connected to a variable flow speed peristaltic pump [no. 2] (Master flex L/S pump, Cole-Parmer) via a three-way valve. The influent solutions are applied onto a plastic filter that evenly distributes the solution over the diameter of the column.

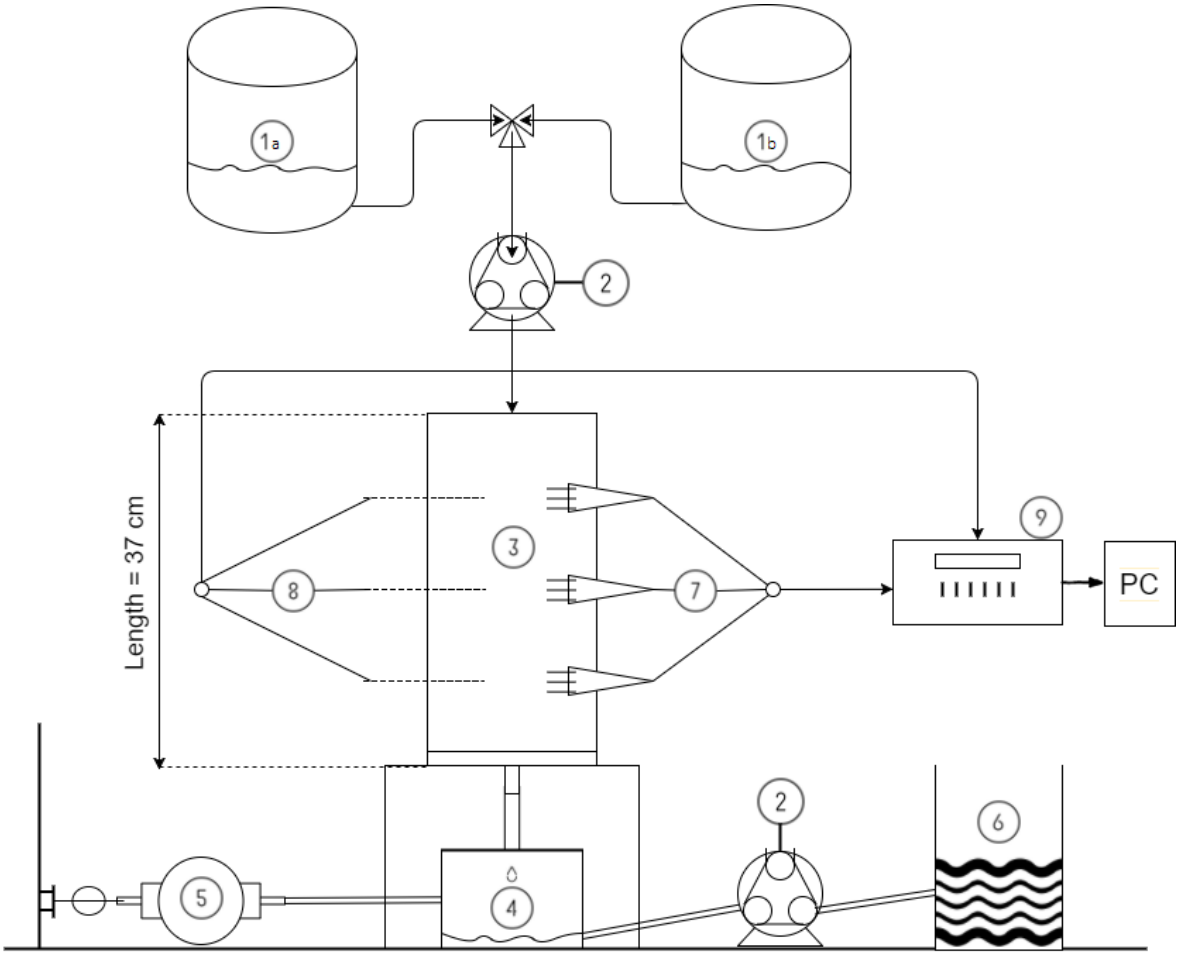

FIGURE 2.1: Schematic of experimental setup, numbers indicating various components

On both sides of the 37-cm-long column [no. 3], sensors are installed [no. 7,8]. The sensors on the left side of the column are tensiometers [no. 8, Rhizo Instruments (Wageningen)]. The tensiometers measure the pressure head at equidistant depth (z=10.5, 18, and 25.5 cm) along the column. On the right hand side, the 5TE sensors [no. 7, Decagon Devices,

Inc., 2008] are inserted at equidistant depth equal to the depth of the tensiometers. Both tensiometers and 5TE-sensors are directly transmitting electrical data to the datalogger. The 5TE sensors measure the permittivity (ϵ), bulk electrical conductivity (σ_b) and temperature (T).

The bottom of the column [no. 3] is connected to a vacuum chamber [no. 4]. This vacuum chamber applies a negative pressure (relative to atmospheric) to the column, simulating unsaturated conditions. The vacuum chamber is also connected to the vacuum regulator and pump [no. 5] for applying the negative pressure. Additionally, the vaccuum chamber [no. 4] is connected to a effluent container [no. 6] by a peristaltic pump [no. 2].

2.2 Materials & measuring equipment

2.2.1 Column

The column itself is a 37 cm long custom-made plexiglas cilinder with a diameter of 9.5 cm. At the sides of the column, holes are situated at depths of 10.5, 18, and 25.5 cm for horizontal accommodation of the sensors. A plastic filter is placed on top of the column to evenly distribute influent solution over the whole radius of the column. The bottom of the column is filtered by a 5 mm thick polyethylene hydrophilic porous membrane (see Section 2.3). The outlet of the column is attached to either a hanging column or vacuum chamber.

2.2.2 Tensiometer

The tensiometer measures the matric water potential relative to the potential in the shaft. A small vacuum chamber, applied by a syringe makes sure that the pore suction pressure in the shaft is near -1 atmosphere. The movement of water through the porous ceramic cup is a function of the pressure difference between the tensiometer and the soil. When there is no more flow through the ceramic cup, the tensiometer is at equilibrium. The actual measurement of pore pressure head is converted to an electrical signal and sent to the datalogger.

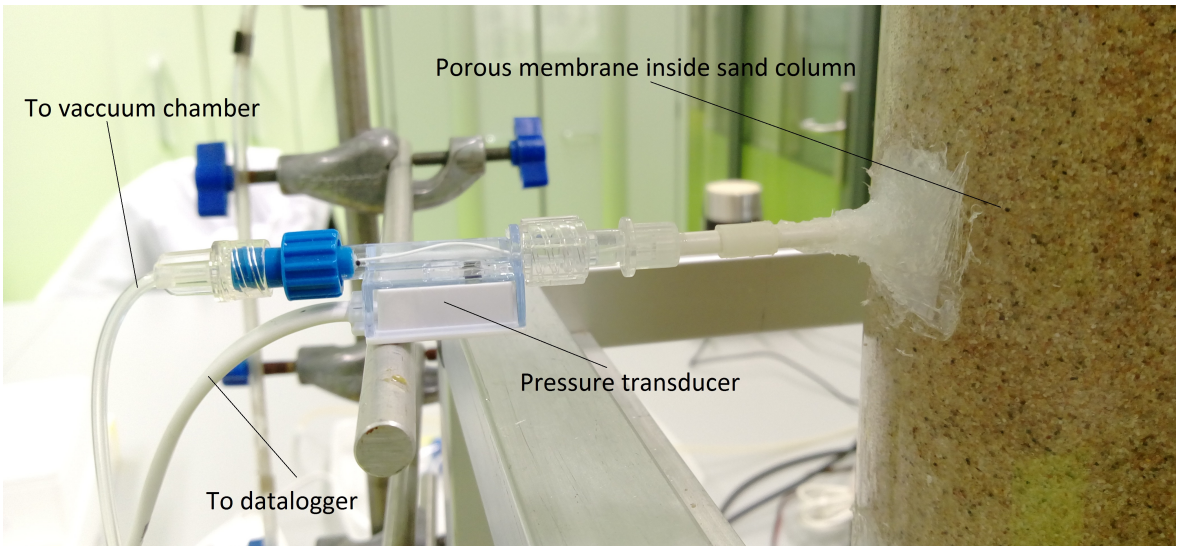

FIGURE 2.2: Tensiometer used for soil moisture pressure measurements inside the column

2.2.3 5TE-sensor

The sensor used for monitoring solute concentration and saturation of the column is a dielectric soil moisture sensor. The 5TE measures the capacitance of the porous medium between the sending and receiving end of the prongs (see Figure 2.3). The bulk electrical conductivity is measured between the two screw arrays on the prongs of the 5TE by applying an alternating electrical current and measuring the resistance between the two arrays (affected by water content, air content, solute concentration in wetting fluid and type of porous medium). The volumetric water content and pore electrical conductivity are respectively estimated by use of the Topp equation ((Topp et al., 1980)) and the linear approach of Hilhorst (2000) to convert bulk EC to pore EC, see Eq. 3.7. Specifications of the 5TE sensor are shown in Table E.1.

$$\theta = 4.3 \times 10^{-6} \times E_a^3 - 5.5 \times 10^{-4} \times E_a^2 + 2.92 \times 10^{-2} \times E_a - 5.3 \times 10^{-2} \tag{2.1}$$

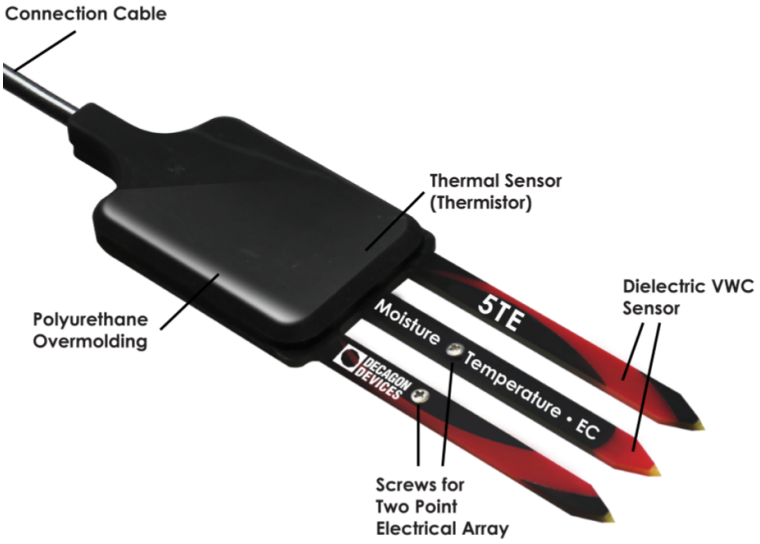

FIGURE 2.3: The 5TE-sensor used in the experiment, figure from Decagon Devices (2016).

2.3 Porous media characteristics

In this study, three different sand-textured porous media have been used. The first porous medium is a coarse-grained sand (S1) with average grain size diameter of 500 μm. The second porous medium is a fine-grained sand (S2) with an average grain size diameter of 215 μm. The third porous medium is a very fine-grained sand with an average grain size diameter of 130 μm. Detailed grain size distribution of S1, S2, and S3 are displayed in Figure 2.4. Saturated conductivity (K_{s1}) of S1 is determined at 69.12 m d^{-1}, whereas the saturated conductivity of S2 (K_{s2}) is significantly less, at 14.41 m d^{-1}, and S3 has a saturated conductivity (K_{s3}) of 3.32 m d^{-1}. Characteristics of the porous media have been outlined in Table 2.1. A statistical analysis of the grain-size data also shows that the sands are all well sorted porous media with similar sorting coefficients (Folk, 1966). Equation 2.2 is used to calculate the sorting of the porous media.

$$\sigma_1 = \frac{\Phi_{84} - \Phi_{16}}{4} + \frac{\Phi_{95} - \Phi_5}{6.6} \tag{2.2}$$

Where Φ is the logarithmic transformation to integers from the grain size data in millimeters. The subscripted number denotes the particle size at that percentile of weight of the sample. The calculation from particle size to Φ is given by Equation 2.3.

$$\Phi = -log_2 d \tag{2.3}$$

Where d is the particle diameter [mm]. The Φ value of the three sands are respectively, 0.198, 0.440, and 0.336 for S1, S2, and S3. Both S1 and S3 fall within the 'very well sorted' category, whereas S2 is placed in the 'well sorted' category.

TABLE 2.1: Porous media characteristics

Porous medium	D_{50} [μm]	K_s [a] [m d^{-1}]	ϕ^a [-]	ρ_s [kg m^{-3}]	ρ_b^a [kg m^{-3}]
S1	500	69.12	0.373	2650	1662
S2	215	14.41	0.306	2650	1839
S3	130	3.32	0.380	2650	1643

[a] For methods of determinating these values, see Section 3.

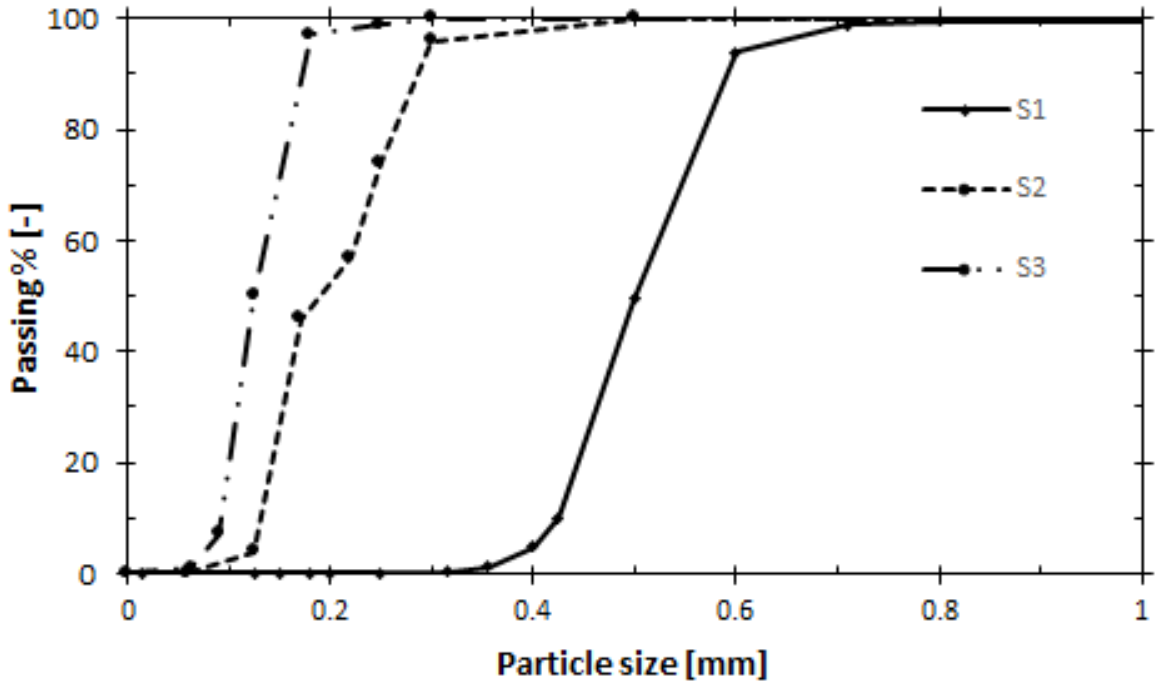

FIGURE 2.4: Grain size distribution of S1

3 Methods

3.1 Saturated flow experiment

The saturated hydraulic conductivity is determined by use of the constant-head method (Fitts, 2002). A column is filled with 10 centimeters of sand, saturated, and a fixed water level is maintained above the surface of the sand. The bottom of the column is covered with a non-woven cloth preventing sand falling from the column, but allowing water to pass through. The outflow from the column is measured over time. Along with the hydraulic head, the height of sand and cross-sectional area, the hydraulic conductivity of the sand is calculated. Figure 3.1 schematically shows the setup used in performing the constant head method.

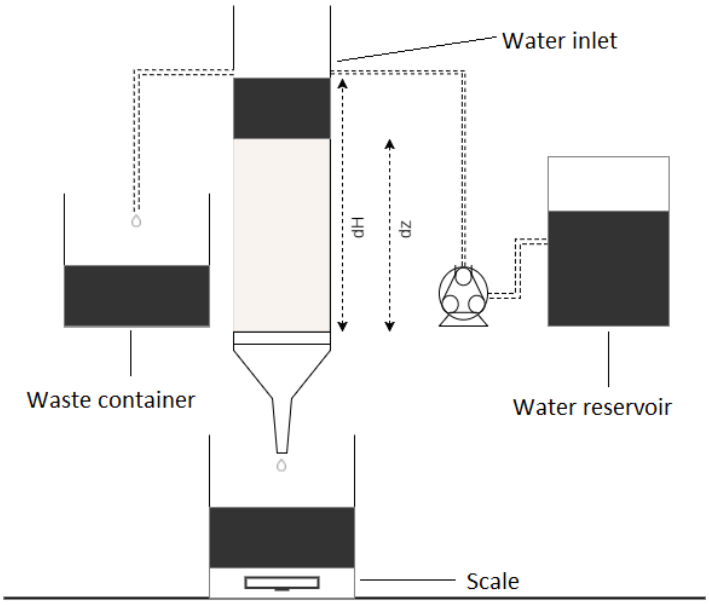

FIGURE 3.1: Schematic illustration of the constant head method

Flow of fluid in a saturated porous medium is analytically described by using Darcy's law for flow ((Fitts, 2002), Eq. 3.1)

$$q = -K\frac{dH}{dz} \tag{3.1}$$

If we rewrite Darcy's law, it is possible to extract the saturated hydraulic conductivity of the sand

$$K = \frac{V}{t_v A}\frac{dz}{dH} \tag{3.2}$$

Where K is the hydraulic conductivity [$L^2\,T^{-1}$], V is the outflow volume [L^3], t is elapsed time during collection of outflow volume [T], A is the area of the column [L^2], dz is the

height of the sand [L] and dH is the total hydraulic head over the height of the sand [L].

The saturated experiment is carried out for different fluxes to indicate the irrelevance of flow velocity to dispersivity for saturated porous media for a constant set of boundary conditions. The three-way valve in Figure 2.1 is switched from DI-water to $CaCl_2$ for a short duration. The pulse of $CaCl_2$ solution is measured by the 5TE sensors and provides data to observe breakthrough curves. These are analytically solved with the CXTFIT program, see Section 3.6 (Toride et al., 1995).

3.2 Unsaturated flow experiment

The unsaturated hydraulic conductivity was initially estimated using retention data and fitting software (RETC, van Genuchten et al. (1991)). Initial estimates of the unsaturated hydraulic conductivity are used as initial condition in the unsaturated experiments. Afterwards, unsaturated hydraulic conductivity has been extracted from pore-water velocity during the unsaturated experiments at unit-gradient. Figure 4.1 shows the relationship between unsaturated hydraulic conductivity and saturation of the porous medium.

Unsaturated flow for our three-dimensional domain will be described by a one-dimensional transient equation since we are only interested in transport of solutes along the vertical axis of the column. This simplification is under the assumption that the domain is completely homogeneous and isotropic. Darcy's law for saturated flow is adjusted for unsaturated domains, this is known as the Richard's equation (Eq. 3.5)

$$\frac{\partial \theta}{\partial t} = \frac{\partial}{\partial z}[K(\theta)\frac{\partial H}{\partial z}] \tag{3.3}$$

Where $\frac{\partial \theta}{\partial t}$ is the partial derivative of θ with time [-], $\frac{\partial}{\partial z}$ the partial derivate with space [-], and $\frac{\partial H}{\partial z}$ the partial derivate of the hydraulic head with space [-]. Since the total head (H) equals the pressure head (h or ψ) plus the elevation head (z), as shown in Eq. 3.4, we can write Eq. 3.3 as Eq. 3.5

$$H = h + z \tag{3.4}$$

$$\frac{\partial \theta}{dt} = \frac{\partial}{\partial z}[K(\theta)[\frac{\partial h}{\partial z} + 1]] \tag{3.5}$$

From the richards equation, it is evident that for a unit hydraulic gradient ($\frac{dH}{dz}$ = 1), the change in saturation is 0. This conditions is a prerequisite for the following unsaturated displacement experiment.

Reproducible unsaturated flow experiments are known to be difficult to establish (Lewis and Sjostrom, 2010; Toride et al., 2003). In pursuance of coherent data for unsaturated flow conditions, a unit hydraulic gradient is fundamental. Unit-gradient conditions are established by changing the influent solution flux at the top and the applied pressure at the bottom, see Figure 2.1. For every degree of saturation there is a specific set of flux and suction (see Figures 4.1 and 4.12). For every saturation, the experiment was conducted twice to verify and improve the precision of the data.

Each experiment, the column is slowly de-saturated to a specific saturation, using DI-water as influent solution. Once unit-gradient conditions are established, i.e. constant volumetric water content (θ) and matric potential (ψ) along the depth of the column, the

unsaturated experiment is initiated. This change in head can be expressed in potential, as seen in Figure 3.2. The three-way valve between the two input solutions is switched to the 0.08 M $CaCl_2$-solution for a given period of time to ensure that the maximum concentration is measured by the 5TE sensors inside the column. Concentration measurement data from three 5TE sensors are consequently solved for the advection-dispersion equation and mobile-immobile equation in CXTFIT to retrieve the dispersion coefficient and mean velocity.

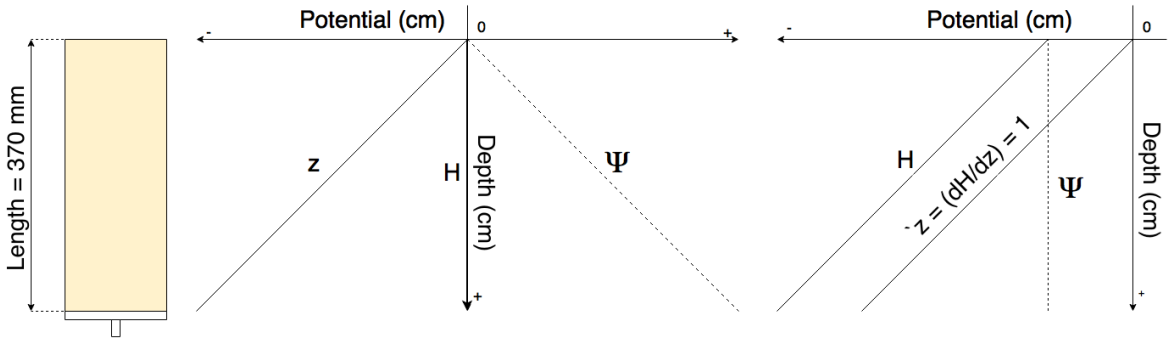

FIGURE 3.2: Schematic illustration of the starting condition (saturated; left), and the initial condition for the unsaturated solute displacement experiment (unsaturated; right). The position of the constant matric potential profile varies with saturation of the porous medium. A lower saturation will shift the matric potential to the left, whereas a higher saturation will move ψ to the right.

3.3 Column preparation

The column used in all of the experiments is described in Section 2.2. Preparation of the column is carried out in a few steps described below. First, the plexiglas column is custom-made to accommodate horizontal insertion of the tensiometers and 5TE-sensors and attached to an inlet and outlet module. A hydrophilic polyethylene porous membrane is fixed at the bottom of the column and glued to the sides of the column to make sure water flows exclusively through the porous membrane.

Before packing the column, all holes designated for insertion of the sensors are taped off, preventing loss of sand during the packing. Packing the column with sand is done according to best-practice packing techniques (Lewis and Sjostrom, 2010; Oliviera et al., 1996). The column is packed by consecutively repeating the following series of actions. First, sand is added with increments of 5 mm height, after which it is firmly pressed on with a custom-made pestle and finally the surface of the sand is slightly scarified with a knife to prevent horizontal layering. The column should now be as homogeneously as possible in terms of vertical porosity distribution.

Most of the oxygen inside the pore space of the sand column is then replaced by flushing it with CO_2-gas for 2 hours. Before inserting the sensors, the sand is wetted with a syringe in order to prevent any loss of sand. Both tensiometers and 5TE-sensor are then horizontally inserted in to the column, any gaps between the opening in the column and the sensors are glued with silicon glue. Saturation of the column with DI-water is slowly done from bottom to top to diminish the possibility of trapping air in enclosed pore spaces.

3.4 Retention data

Retention data of porous media are important to understand behaviour of fluids and solutes during unsaturated conditions. Retention data for the porous media have been determined by use of the HYPROP© device (UMS, Munich, Germany) displayed in Figure 3.3. HYPROP uses a modification of Wind's evaporation method (Schindler et al., 2010), combining change in mass and matric potential to create a retention curve.

Packing of the porous media for retention data determination is done in a 250 cm^3 stainless steel soil ring, covered by a cloth on the bottom and flattened at the top. The soil core is saturated over night, through the cloth-covered bottom of the soil ring in a container filled with de-gassed DI-water. The level of the water is slowly increased over time until it is 5 mm below the top of the soil core. The saturated soil core is subsequently inserted onto the sensor unit (Figure 3.3). The core and sensor unit are entirely fixed onto a balance, measuring the weight loss due evaporation over time. A connection from the pressure transducer to the PC transfers matric potential data from two tensiometers at different depths in the core (see Figure 3.3). Both change in mass and matric potential of the porous media are subsequently used to construct a moisture retention curve, see Figures 4.12 and 4.13 in Section 4 for the retention curve of S1 and S2. In turn, the retention data is solved with the van Genuchten (1980) Equation

$$\theta(h) = \theta r \frac{\theta s - \theta r}{[1 + |\alpha^* h|^n]^m} \tag{3.6}$$

Where θ is the volumetric water content as a function of matric suction [L^3 L^{-3}], θ_r and θ_s respectively the residual and saturated volumetric water content [-], h the matric suction [L], and α^*, n, and m are the van Genuchten parameters [-].

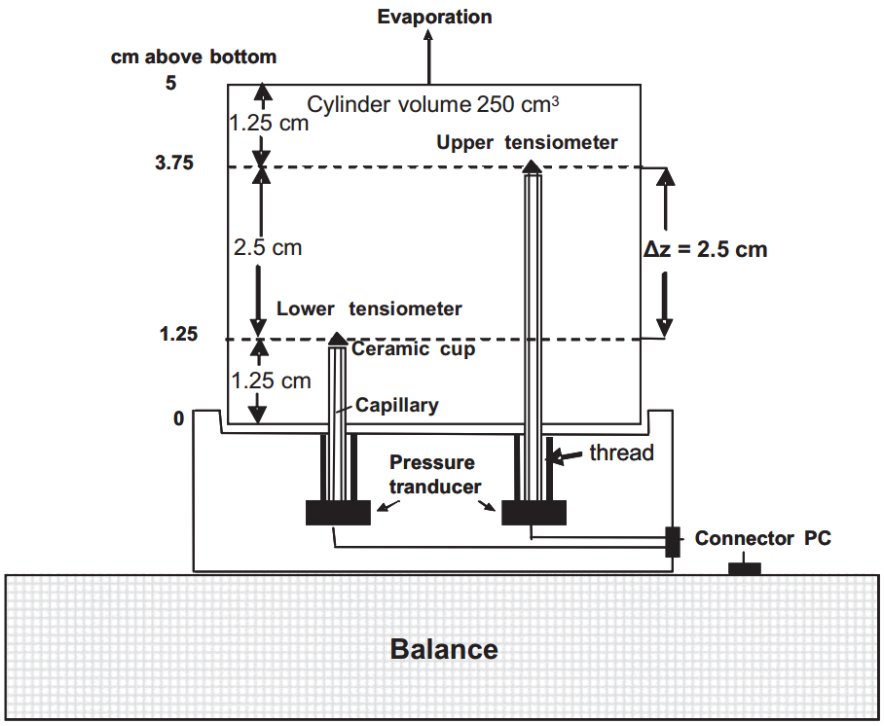

FIGURE 3.3: Schematic figure of the HYPROP device for measuring retention data. Figure reproduced with permission from Schindler et al. (2010)

3.5 Conductivity measurements

5TE-sensors measure EC_b, whereas we are interested in pore-water concentration values. Calculations involving conversion of bulk EC to pore EC prove to be subject to either specific sets of conditions or inaccurate (Hilhorst, 2000). However, a linear distribution between concentration of the solute and the measured EC_b is a fair assumption for low concentration differences (0-0.1M).

Initially, the pore-water electrical conductivity was calculated from bulk electrical conductivity measurements (Hilhorst, 2000).

$$EC_p = \frac{E_p * EC_b}{E_b - E_{b0}} \tag{3.7}$$

Where EC_p is the pore electrical conductivity [$\mu S\ cm^{-1}$], E_p is the real portion of the dielectric permittivity of the soil pore water [-], EC_b denotes the bulk electrical conductivity of the soil [$\mu S\ cm^{-1}$], E_b is the dielectric permittivity [-] and E_{b0} is the dielectric permittivity of the dry soil [-].

This equation uses the permittivity as a proportionality for varying saturation to convert bulk electrical conductivity (EC_b) to pore electrical conductivity (EC_p). However, results showed that permittivity of the soil is not only a function of water content. The amount of dissolved solutes in the fluid had a considerable effect on the permittivity as well. Therefore, Equation 3.7 is not valid (see Appendix B).

Hence, calibration curves must be developed to relate EC_b measurements to the concentration of the input solution. The EC_b-c calibration curves have been developed for each sensor to accurately describe a relationship between the bulk EC and the solution EC. Solution EC (EC_p) is linearly related to concentration of the solution, therefore we can relate EC_b to c. However, this holds only under the assumption that θ is constant throughout the experiment. The previous can be described in a simple equation in the form of

$$c(x,t) = A_0 EC_b(x,t) + B_0 \tag{3.8}$$

Where for each individual sensor there is a specific set of constant A_0 and A_0. The calibration curves are shown in Figure A.1 in Appendix A.

3.6 Data analysis

This chapter covers the analysis of the data acquired through experiments. Numerical fitting techniques used by the CXTFIT program provide a clear estimate of the pore-water velocity and hydrodynamic dispersion coefficient. Initial estimates of the pore-water velocity are calculated through measured flux data during the experiment. Results are based on the fitted pore-water velocity value. Both conditions give rise to the assumption that volumetric water content is equal throughout the column, which was a prerequisite for unit-gradient flow.

3.6.1 Advection-Dispersion model

One of the solution applied to the experimental data is the advection-dispersion equation (ADE). Using Equation 1.1 it simulates the spread of solutes based upon advection and hydrodynamic dispersion as well as retardation due to partitioning of solutes between solid and fluid phase in a one-dimensional line. Since we use a conservative tracer, retardation is neglected. Although the flow domain in this study is three-dimensional, we assume

isotropic and homogeneous conditions in the porous medium. This allows for a simplification in terms of modeling concentration through time and space. The one-dimensional ADE model therefore simulates the average concentration of the plane perpendicular to the flow direction. In general, the ADE model is sufficiently accurate for a relatively high mobile water content (θ_m). However, in unsaturated soils with a lower saturation, different conditions may arise. In order to quantify the conditions in unsaturated soils where the ADE analytical solution may not be accurate enough, we also employ a Mobile-Immobile model (see Section 3.6.2).

3.6.2 Mobile-Immobile model

At lower saturation, near residual water content, the mobile water content decreases and an alternative approach to to the ADE model may better describe the characteristics of flow in the porous medium. The Mobile-Immobile (MIM) takes into account immobile portions of the flow region to accommodate a better fit of the elongated concentration profile.

The two-region non-equilibrium transport model for a homogeneous soil in one dimension, without adsorption to the solid phase and degradation (conservative solutes) is described by (Toride et al., 1995):

$$\theta_m \frac{\partial c_m}{\partial t} = \theta_m D_m \frac{\partial^2 c_m}{\partial z^2} - q \frac{\partial c_m}{\partial z} \tag{3.9}$$

$$\theta_{im} \frac{\partial c_{im}}{\partial t} = \omega (c_m - c_{im}) \tag{3.10}$$

Where θ_m and θ_{im} are respectively the mobile and immobile fractions of total volumetric water content [-], c_m and c_{im} are the concentration of solutes in respectively the mobile and immobile fraction [M L^3], D_m is the dispersion coefficient of the mobile region [L^2 T^{-1}] and ω is the first-order transfer coefficient between the mobile and immobile region [T^{-1}].

Initial conditions for the MIM-model are similar to the ADE-model. However, in addition to the velocity and dispersion coefficient, MIM also requires initial conditions for the partitioning between the mobile and immobile regions β [-], as well as a first-order transfer coefficient between the two regions, ω [T^{-1}]. As a result, this model takes in account two region flow with exchange of solutes described as a first-order process.

TABLE 3.1: Advection-Dispersion & Mobile-Immobile conditions

I.C./B.C.	Advection-Dispersion model[a]	Mobile-Immobile model[a]
I.C. 1	c(z,0) = 0 (c_0)	c(z,0) = 0 (c_0)
I.C. 2	c(t,z) - $\alpha \frac{dc}{dz}$ = c_0	c(t,z) - $\alpha \frac{dc}{dz}$ = c_0
B.C. 1	$\frac{dc(\infty,t)}{dz}$ = 0	$\frac{dc(\infty,t)}{dz}$ = 0
B.C. 2	c(t,z) - $\alpha \frac{dc}{dz}$ = c	c(t,z) - $\alpha_m \frac{dc}{dz}$ = c
Initial v	from measured outflow	-
Initial β	-	(0.3 <β <0.99)
Initial ω	-	0.01

[a] Where c_0 is the background concentration (DI-water) and c the calculated concentration

4 Results

4.1 Unsaturated hydraulic conductivity

The unsaturated hydraulic conductivity was first estimated using retention data and fitting software (RETC, (van Genuchten et al., 1991)), and later determined with pore-water velocity from unsaturated experiments. Figure 4.1 shows the hydraulic conductivity as a function of saturation as a result of the unsaturated experiments. The relation is plotted on a semi-logarithmic graph to visualize the exponential nature of the relation.

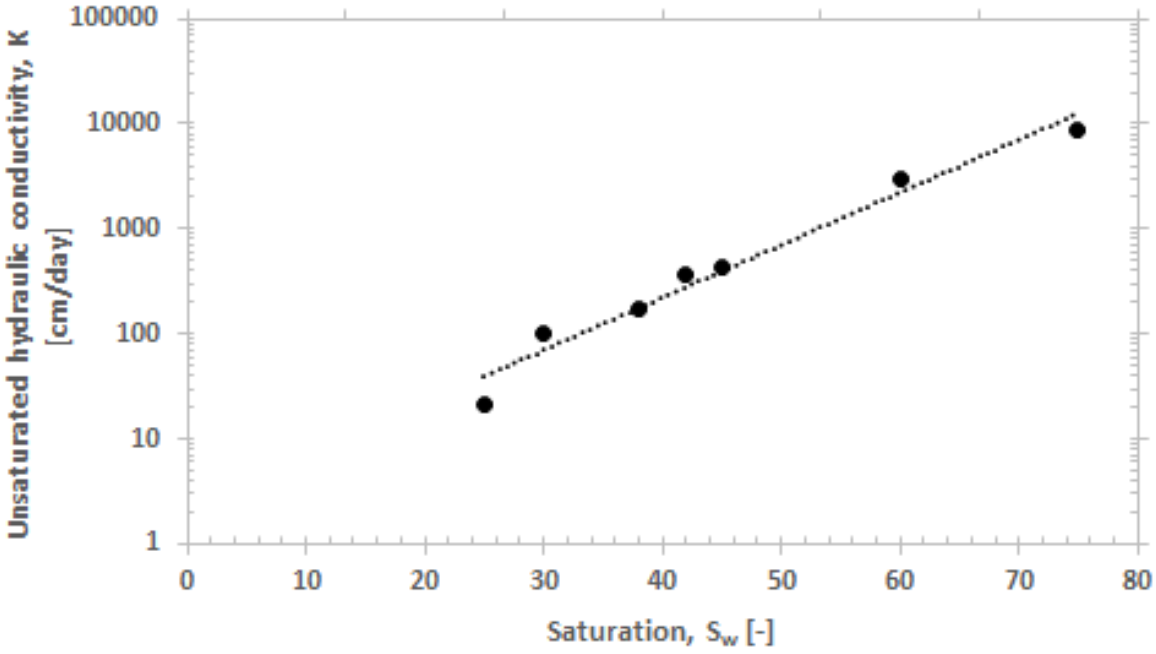

FIGURE 4.1: Hydraulic conductivity as a function of saturation for S1

4.2 Analysis of experimental data

4.2.1 Modelling by Advection-Dispersion model

Breakthrough curves in Figures 4.2, 4.3, and 4.4 show the results from the experiments at different saturation of the porous medium. For all breakthrough curves, the concentration has been normalized to the maximum concentration (concentration of influent $CaCl_2$-solution) by the following equation.

$$C_n = \frac{C - C_0}{C_1 - C_0} \tag{4.1}$$

Where C_n is the normalized concentration [-], C is the measured concentration [M L^3], C_1 is the input concentration [M L^3], and C_0 is the initial concentration [M L^3].

TABLE 4.1: Experimental data from saturated flow experiments for three porous media, all values are from the middle section of the column (z = 18 cm)

	#	Saturation	ϑ [-]	q [cm min^{-1}]	v [cm min^{-1}]	D [cm^2 min-1]	α [cm]	r^2
S1	1	1.00	0.365	0.067	0.184	0.007	0.04	0.9996
	2	1.00	0.365	0.126	0.344	0.019	0.05	0.9990
S2	3	1.00	0.292	0.271	0.927	0.025	0.03	0.9999
	4	1.00	0.292	0.027	0.091	0.002	0.02	0.9960
	5	1.00	0.292	0.130	0.445	0.014	0.03	0.9997
S3	6	1.00	0.357	0.088	0.245	0.002	0.01	0.9996
	7	1.00	0.357	0.123	0.345	0.003	0.01	0.9971
	8	1.00	0.357	0.156	0.438	0.004	0.01	0.9980

Table 4.1 shows the results from modeling saturated flow experiment data with the ADE through the porous media. Both velocity and dispersion coefficient are point-averaged values representing an average value for the entire flow domain at the particular location (depth = 18 cm). Interestingly, there is a direct proportional correlation between the saturated dispersivity and the average grain size diameter of the porous media (see Tables 4.1 and 2.1). However, it seems that this only holds if the variance of the particle size distribution of the sands are similar.

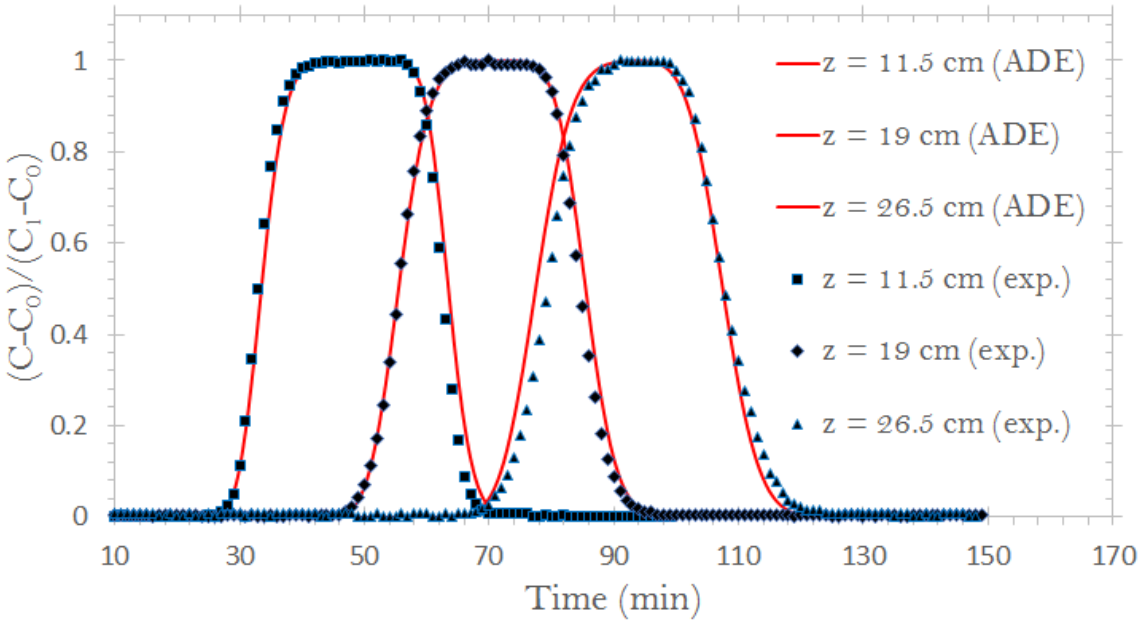

FIGURE 4.2: Breakthrough curves under saturated condition (S_w=1) at three locations (11.5, 19 and 26.5 cm) from inlet. Flux = 0.341 cm min^{-1}. Points indicate data, lines indicate fit by ADE-model in CXTFIT

Figure 4.2 displays the breakthrough curves for three different locations (z=11.5, 19 and 26.5 cm) for the saturated porous medium. The graphs clearly show a Gaussian distribution, indicating that there are few irregularities in the flow paths and a high mobile water content. Each individual location is shown to have the same dispersivity **reference to table with all the data for all experiments**, showing that the sand in the column is distributed quite homogeneous and has a porosity-profile that is equal at all depths. Interestingly, the

dispersivity increases slightly with increasing travel distance. This is arguably due to the scale effect of dispersion (Khan and Jury, 1990).

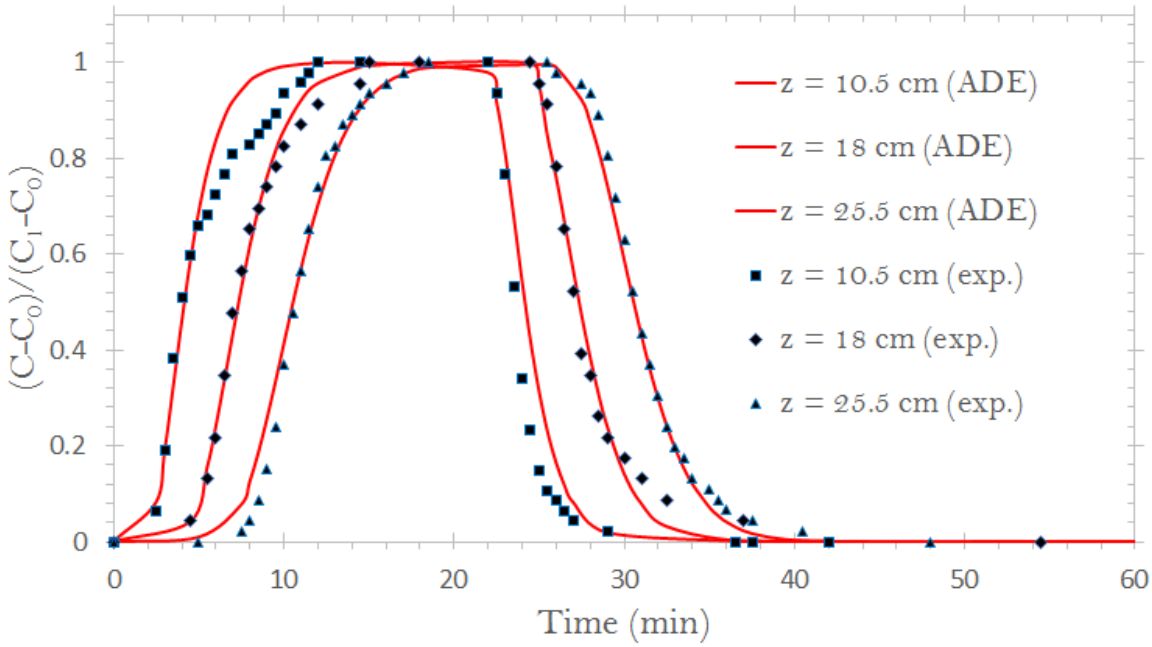

FIGURE 4.3: Breakthrough curves under unsaturated condition (S_w=0.5) at three locations (10.5, 18 and 25.5 cm) from inlet. Flux = 0.420 cm min^{-1}. Matric potential = -16.7±0.5 cm. Points indicate data, lines indicate fit by ADE-model in CXTFIT

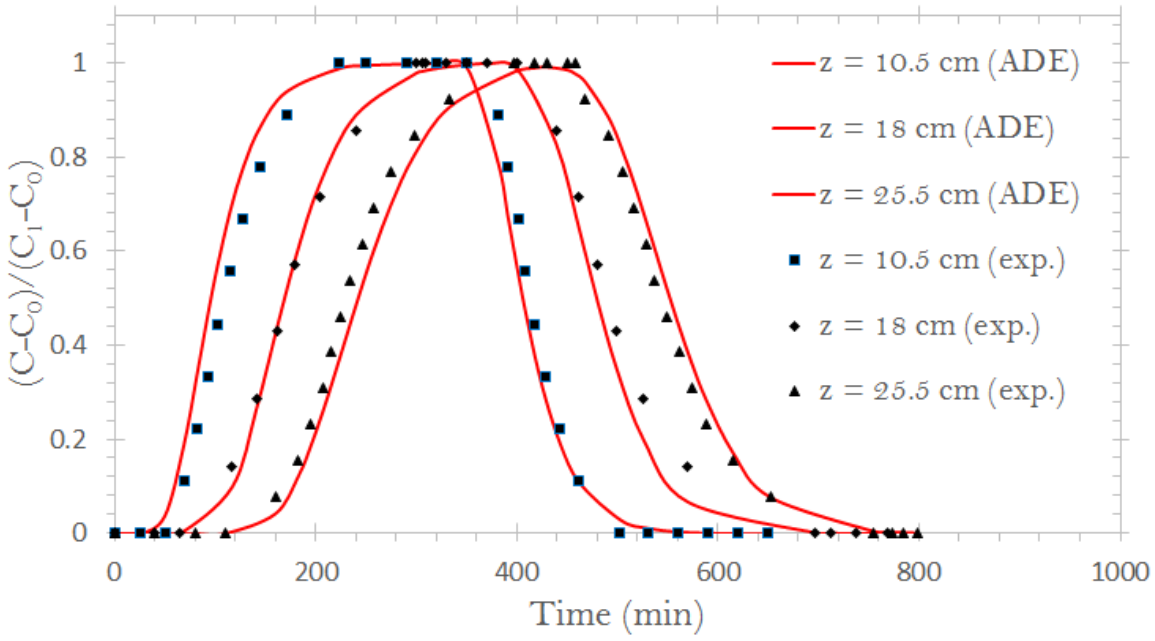

FIGURE 4.4: Breakthrough curves under unsaturated condition (S_w=0.25) at three locations (10.5, 18 and 25.5 cm) from inlet. Flux = 0.010 cm min^{-1}. Matric potential = -23.35±0.3 cm. Points indicate data, lines indicate fit by ADE-model in CXTFIT

The breakthrough curves shown in figure 4.3 show a different concentration profile than for the saturated condition in figure 4.2. The shape of the breakthrough curve shows signs of immobile water content and a higher dispersion coefficient. In the rising limb of the breakthrough curve a flattening near the top can be seen. Whereas in the falling limb, there is evidence of tailing. The sensor at a depth of 10.5 cm shows measurements that deviate from what is expected at t = 6 minutes to t = 12 minutes. This is most likely due to some heterogeneities at the top of the column.

The breakthrough curves for a saturation (S_w) of 0.25, shown in Figure 4.4 Still show quite a large effect of dispersion to the concentration distribution over time. However, dispersivity for this saturation is lower than for a saturation of 0.5 (see Figure 4.3). The shape of the curves show a similar distribution as the other unsaturated breakthrough curve, including considerable tailing as an effect of stagnant zones or immobile water content.

Interestingly, breakthrough curve data from the furthest position show an elevated velocity with respect to the first two measurement depths, as well as a lower dispersion coefficient. For the latter, this is contrary to the expected increase in dispersion coefficient as result of scale-effects (Gelhar et al., 1992). Figure 4.5 shows a possible interpretation of the phenomena that caused variation in the measurements at 5TE-3 sensor. The non-unit gradient conditions near the bottom of the column likely influence the dispersion coefficient due to a higher water content, as well as the velocity due to a higher hydraulic gradient.

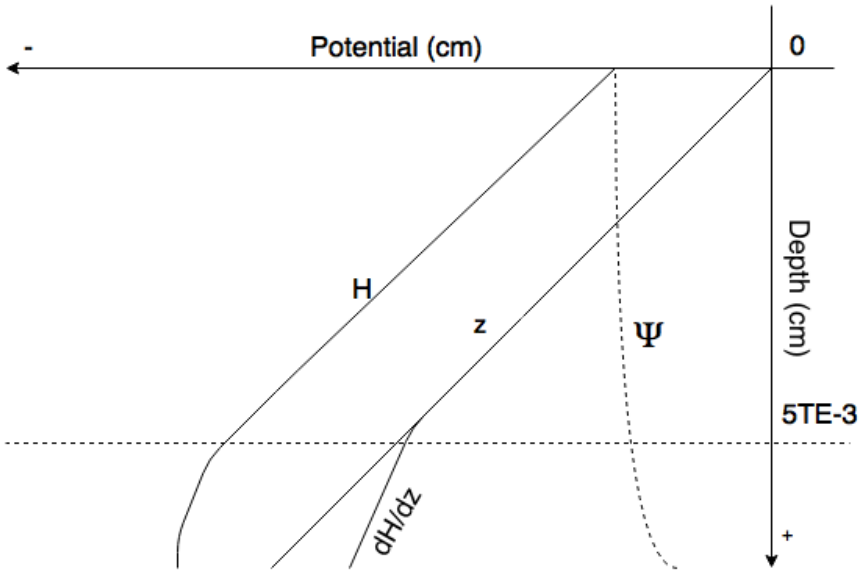

FIGURE 4.5: Schematic pressure diagram showing the position of furthest 5TE sensor from inlet. non-unit gradient conditions below the sensor influence the dispersion coefficient.

4.2.2 Modelling by Mobile-Immobile model

In an effort to increase the accuracy of the model results from the experimental data, we employ another model, supposedly more suitable for modelling transport of solutes under unsaturated conditions. The mobile-Immobile model considers a division in mobile and immobile water content and applies an exchange parameter between the two regions. Results in this section show the mobile water content as a function of the saturation, as well as a dispersivity-saturation plot for the mobile portion of the domain. The results are distinctively different than the results from the advection-dispersion model. The mobile-immobile

model shows that the dispersivity for the mobile region increases with decreasing saturation up to a saturation of 0.35 (Figure 4.6 and Table 4.2), whereas the ADE-model has a peak dispersivity at a saturation of 0.43 (Figure 4.8 and Table 4.3). However, the mobile water content decreases drastically after an intermediate saturation (Figure 4.7). Therefore, the overall dispersive behaviour for low saturation of the porous medium is lower with the MIM-model than with the ADE-model.

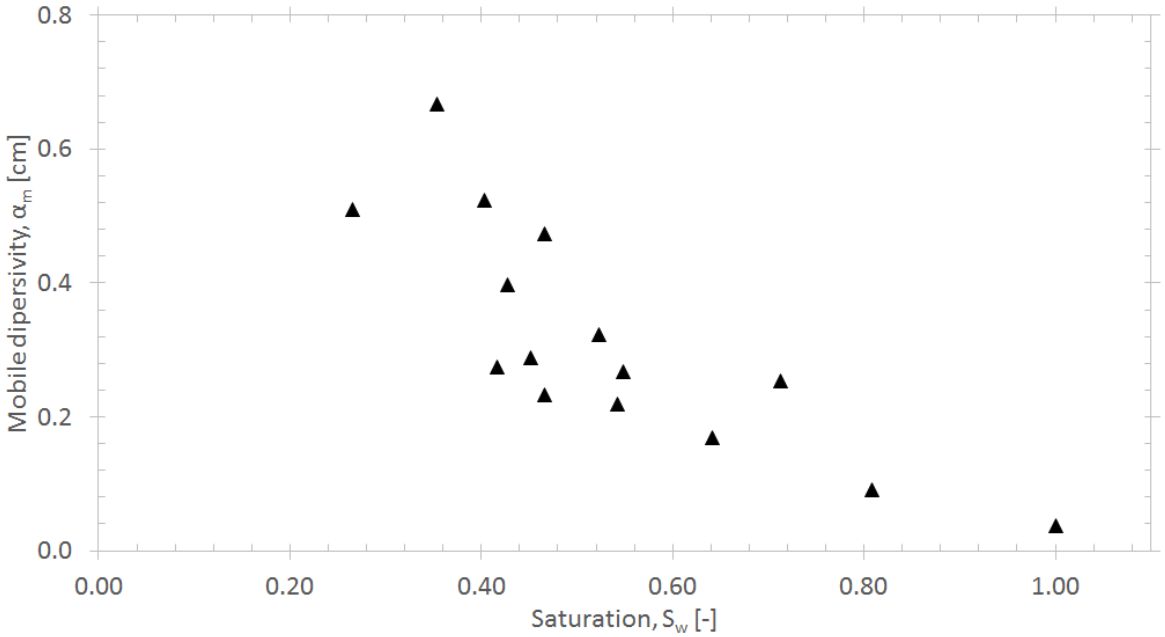

FIGURE 4.6: Shows the Mobile dispersivity (α_m) as a function of saturation, the data is from the middle of column (z = 18 cm)

The mobile water content of the sand is estimated through the MIM equations (Eq. 3.9 & 3.10) by a least squares regression analysis. The mobile water content is defined as the fraction of water content that is in flow, as shown in Equation 4.2.

$$\beta = \frac{\theta_m}{\theta} \tag{4.2}$$

where θ is defined as $\theta_m + \theta_{im}$. whats interesting about the mobile water content is that with decreasing saturation, it only decreases. The amount of stagnant water zones is therefore larger in a low-saturation flow domain, according to the MIM model output.

Padilla et al. (1999) showed that greater velocities enhance the mass transfer rates by causing faster mixing between the two regions. Data by this study does not show a significant trend in mass transfer rates. However, the lowest saturations

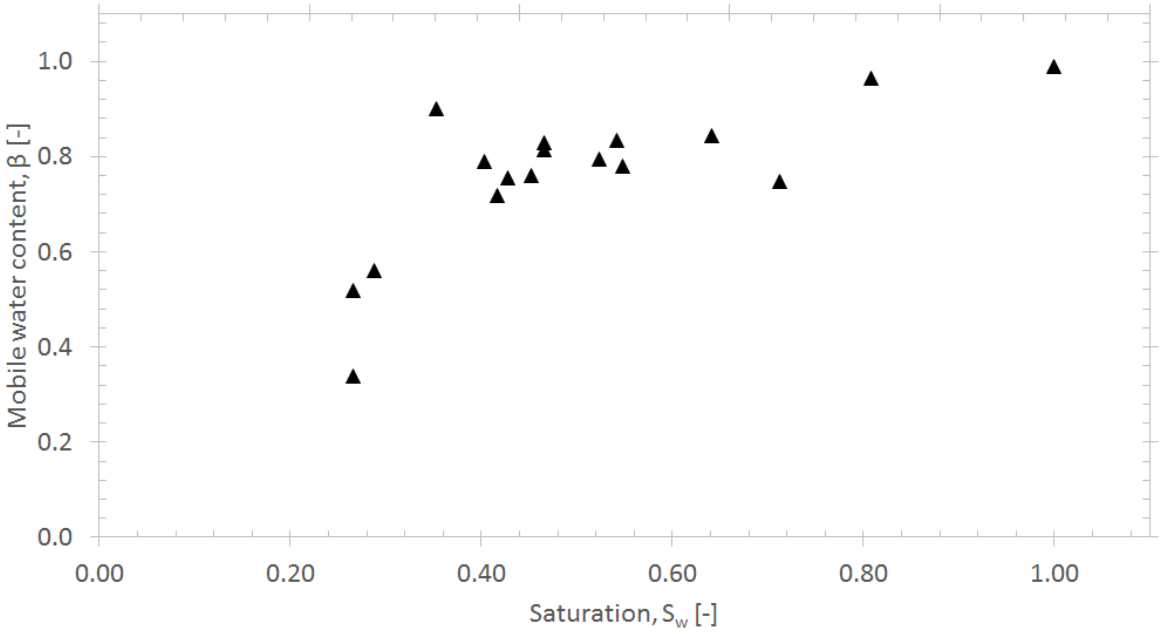

FIGURE 4.7: Shows the Mobile water content fraction (β) as a function of saturation, the data is from the middle of column (z = 18 cm)

TABLE 4.2: MIM-model results

	#	Saturation	ϑ [-]	q [cm min^{-1}]	v_m [cm min^{-1}]	D_m [cm^2 min^{-1}]	β [-]	ω [min^{-1}]	α_m [cm]	r^2
S1	1	0.27	0.097	0.00	0.096	0.049	0.338	0.464	0.51	0.999
	3	0.35	0.129	0.04	0.386	0.258	0.900	0.012	0.67	0.998
	4	0.40	0.147	0.09	0.741	0.389	0.790	0.056	0.52	0.999
	5	0.42	0.152	0.08	0.742	0.204	0.717	0.079	0.27	0.999
	6	0.43	0.156	0.14	1.182	0.470	0.754	0.039	0.40	0.997
	7	0.45	0.165	0.14	1.078	0.311	0.759	0.040	0.29	0.996
	8	0.47	0.17	0.30	2.117	1.002	0.829	0.036	0.47	0.990
	9	0.52	0.191	0.38	2.499	0.806	0.795	0.045	0.32	0.997
	10	0.55	0.2	0.49	3.134	0.837	0.780	0.029	0.27	0.993
	11	0.64	0.234	1.02	5.171	0.876	0.844	0.043	0.17	0.998
	14	1	0.365	0.12	0.344	0.013	0.990	0.023	0.04	0.999

4.3 Analysis of saturation dependency

The primary goal of this study is to quantify the saturation dependency of dispersivity. For S1, the saturated and unsaturated dispersivity has been extensively measured over the entire range of saturation. As a result, Figure 4.8 shows the calculated dispersivity from each breakthrough curve for 5TE-1 (z=10.5 cm) and 5TE-2 (z=18 cm). Results show indisputable evidence for a non-monotonic behaviour of dispersivity as a function of saturation. For high saturation, dispersivity is low, since the variation in flow paths is minimal for (near-)saturated flow. when a soil is desaturated towards intermediate saturation, dispersivity increases, with a maximum of 1.32 cm at a saturation of 0.43. Figure 4.9 shows a schematic representation of intermediate saturation (middle figure). In this figure, both the larger (macro-) as well as smaller (micro-) pores are partially saturated. As a result, the relatively high variability of flow paths in the porous medium increases the dispersion coefficient.

TABLE 4.3: Experimental data from unsaturated flow experiments for porous medium S1, at depth z = 18 cm (5TE-2)

	#	Saturation	ϑ [-]	q [cm min-1]	v [cm min -1]	D [cm2 min-1]	α [cm]	r^2
S1	1	0.27	0.097	0.010	0.098	0.078	0.79	0.995
	2	0.29	0.105	0.023	0.214	0.205	0.96	0.998
	3	0.35	0.129	0.052	0.401	0.385	0.96	0.997
	4	0.40	0.147	0.111	0.755	0.893	1.18	0.996
	5	0.42	0.152	0.115	0.760	0.875	1.15	0.995
	6	0.43	0.156	0.195	1.251	1.652	1.32	0.991
	7	0.45	0.165	0.190	1.149	1.294	1.13	0.987
	8	0.47	0.170	0.371	2.185	2.186	1.00	0.988
	9	0.52	0.191	0.490	2.565	2.717	1.06	0.994
	10	0.55	0.200	0.687	3.435	2.887	0.84	0.978
	11	0.64	0.234	1.246	5.325	2.817	0.53	0.992
	12	0.71	0.260	1.868	7.186	3.930	0.55	0.978
	13	0.81	0.295	2.533	8.587	0.853	0.10	0.999
	14	1.00	0.365	0.126	0.344	0.019	0.05	0.999

Furthermore, for S_w <0.43, dispersivity decreases. In low saturation of a porous medium ($S_{w,r}$ <S_w < 0.43), macropore flow is not dominant (or is completely absent) in displacement of fluids (see Figure 4.10). Micropore flow becomes the dominant flow regime (see top figure in Figure 4.9). Inside the smaller pore spaces, there is a higher capillary interaction with the solids. Therefore, pores in these flow paths are able to retain water, yet the wetting phase remains transient in terms of flow through these pores, largely due to the applied suction at the bottom of our flow domain. Since flow is limited to generally fewer flow paths (and more homogeneous flow regimes), the variation in flow becomes less significant. These factors influence the total dispersion coefficient for a specific saturation.

For porous medium S1, an α-S_w (Figure 4.8) plot describes the variation of dispersivity for that porous medium with a specific set of characteristics. However, it would be useful to quantify these results as a function of the characteristics of the porous medium. Possible ways to quantify the α-S_w relation would be to make it dependent on physical properties such as mean particle size, average pore radius, or variance of particle sizes.

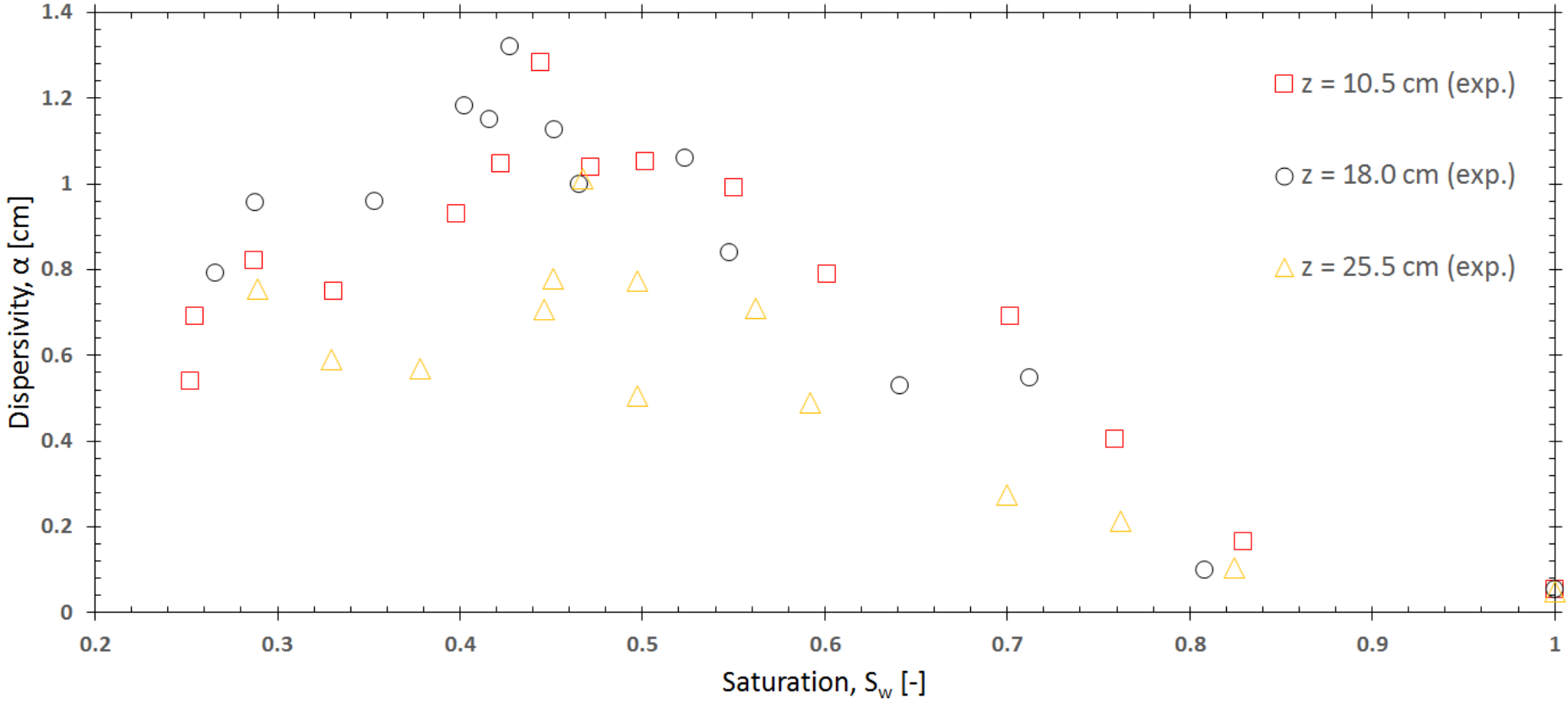

FIGURE 4.8: Dispersivity distribution as a function of saturation, data points indicating dispersivity for a certain saturation for depths of 10.5, 18, and 25 cm

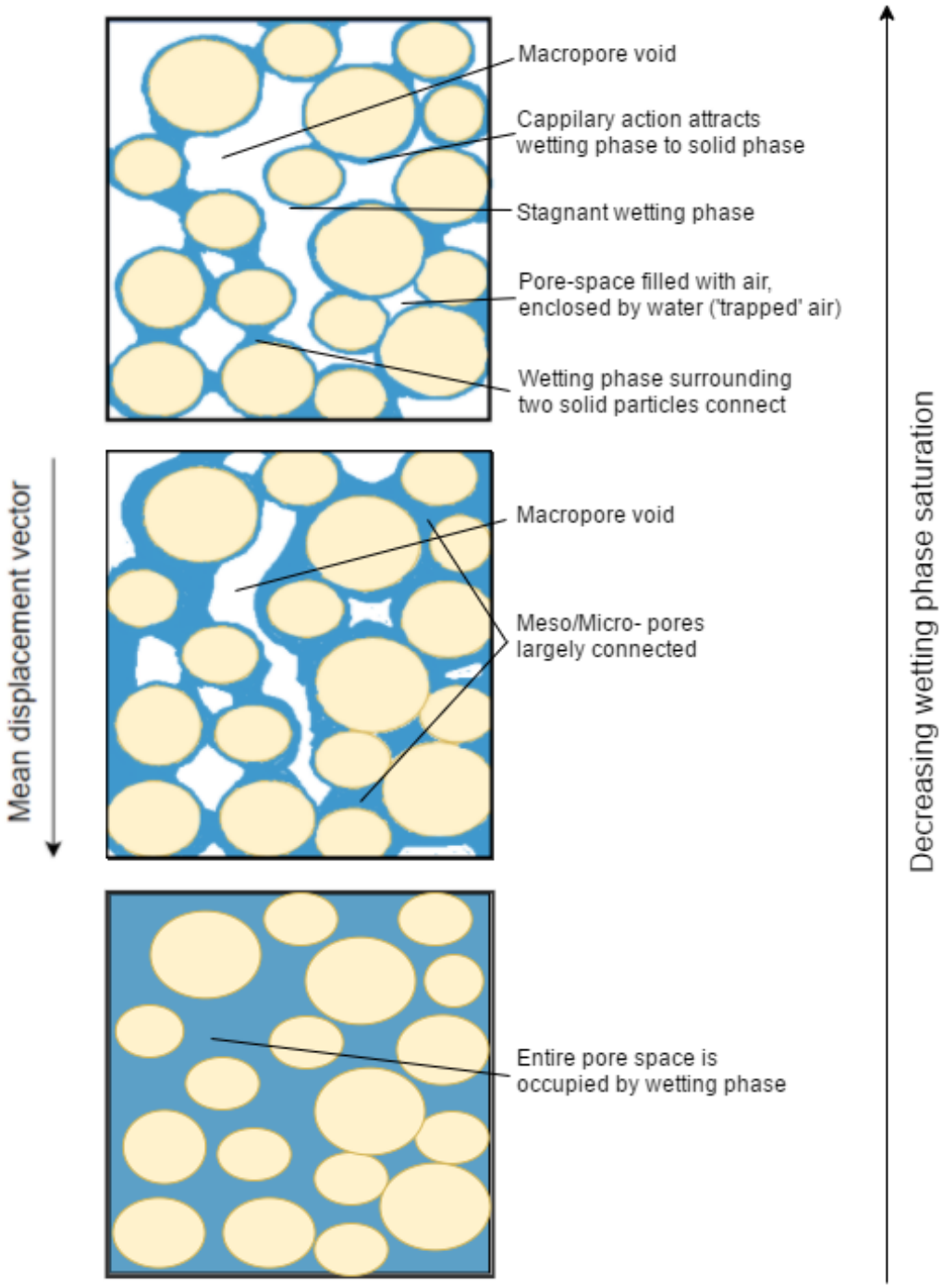

FIGURE 4.9: Pore space distribution under varying conditions. top: (near-) residual saturation; middle: intermediate saturation; bottom: saturated.

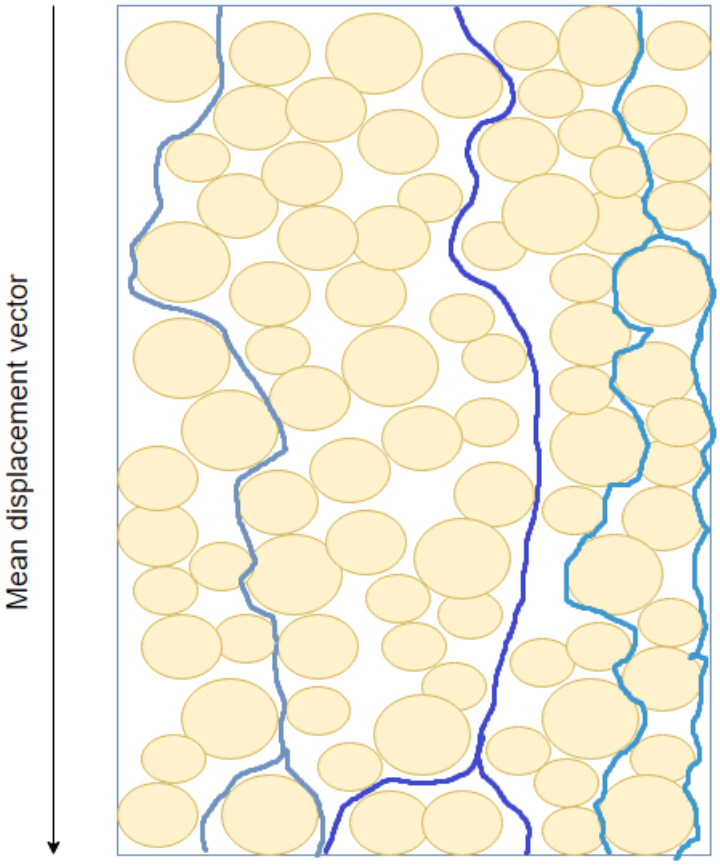

FIGURE 4.10: Representation of porous medium, slightly exaggerated differences between pore radii to illustrate hydrodynamic dispersion under unsaturated conditions. Left: mesopore flow; middle: macropore flow; right: micropore flow.

Despite the non-monotonic trend of α with regard to saturation at all three depths, not all measurements show the same distinct behaviour. Data from 5TE-3 shows a non-monotonic α-S_w relation, however, the shape is slightly flattened with respect to data from 5TE-1 and 5TE-2, i.e. the maximum dispersivity is lower at 5TE-3. Possible explanations of this phenomenon are explained in Section 5. Results from all three sensors, including a fitted function of the data is shown in Appendix C. The function describing the α-S_w relation is of a gaussian nature (Eq. 4.3).

$$\alpha(S_w) = ae^{-(\frac{S_w-b}{c_0})^2} \tag{4.3}$$

Where α is the dispersivity [L], S_w is the wetting phase saturation [-], and a, b, and c_0 are constants.

The constant a, b, and c_0 are respectively 1.14, 0.419, and 0.280 When solving for the data acquired at the center of the flow domain of porous medium S1 (z = 18 cm). The most interesting shape parameters of Eq. 4.3 are a and c_0. These parameters influence the slope of the curve as well as the maximum value. Therefore, if causality between for example average grain size diameter (D_{50}) and maximum unsaturated dispersivity of a porous medium can be proven, the equation is suitable to estimate entire dispersivity ranges across a wide range

of homogeneous sandy porous media. Consequently, this has interesting implications for unsaturated zone modelling.

4.4 Analysis of scale-effect

Dispersion coefficient increase with scale of domain has been proven to in field-scale experiments (Gelhar et al., 1992). A study by (Khan and Jury, 1990) shows indifferent results, not proving evident scale effects of dispersivity due to domain length or amount of influent flux. Figure 4.11 shows the dispersion coefficient result of 5TE-2 as a fraction of the dispersion coefficient of 5TE-1. The result shows an overall increasing trend in the dispersion coefficient. The comparison between 5TE-3 and 5TE-2 is not carried out due to the non-unit gradient near the third sensor. Therefore, we cannot make a reasonable comparison between these two measurement points.

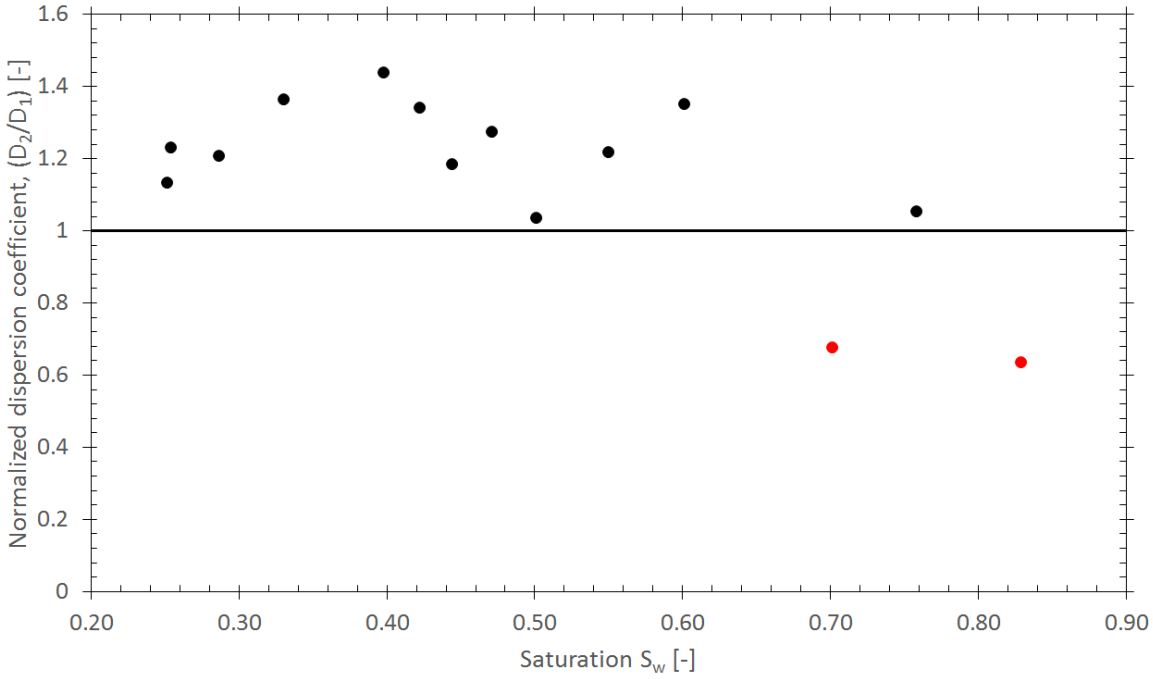

FIGURE 4.11: Scale effect of the dispersion coefficient

4.5 Retention data

Retention data of S1 is displayed in Figure 4.12. The retention data shows that the porous medium has a narrow range of particle sizes. As well, it shows that the effective range of soil water potential extends from 0 to -25 cm.

Figure 4.13 shows the retention data and van Genuchten fit for the porous medium S3. The van genuchten parameters are shown in the figure. The retention curve suggests this sand has more or less the same variation in grain sizes. However, due to the much finer particles, a higher suction has to be applied for the medium to desaturate.

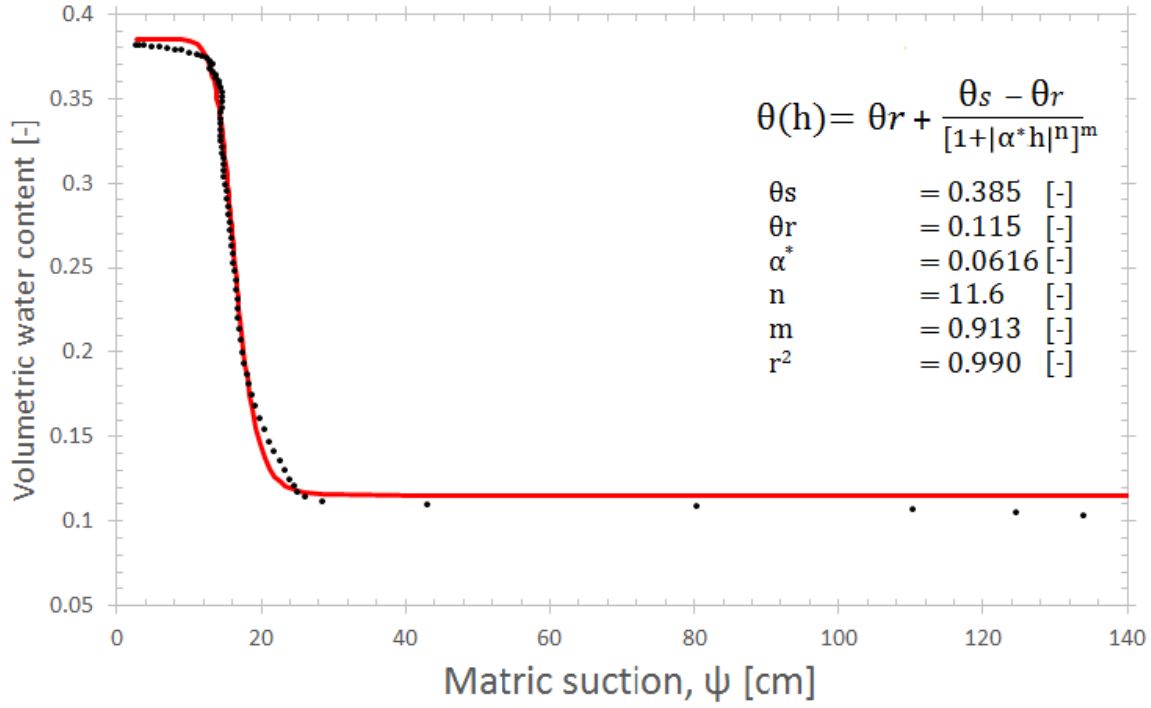

FIGURE 4.12: Retention curve of S1, fitted with the van Genuchten equation (van Genuchten, 1980).

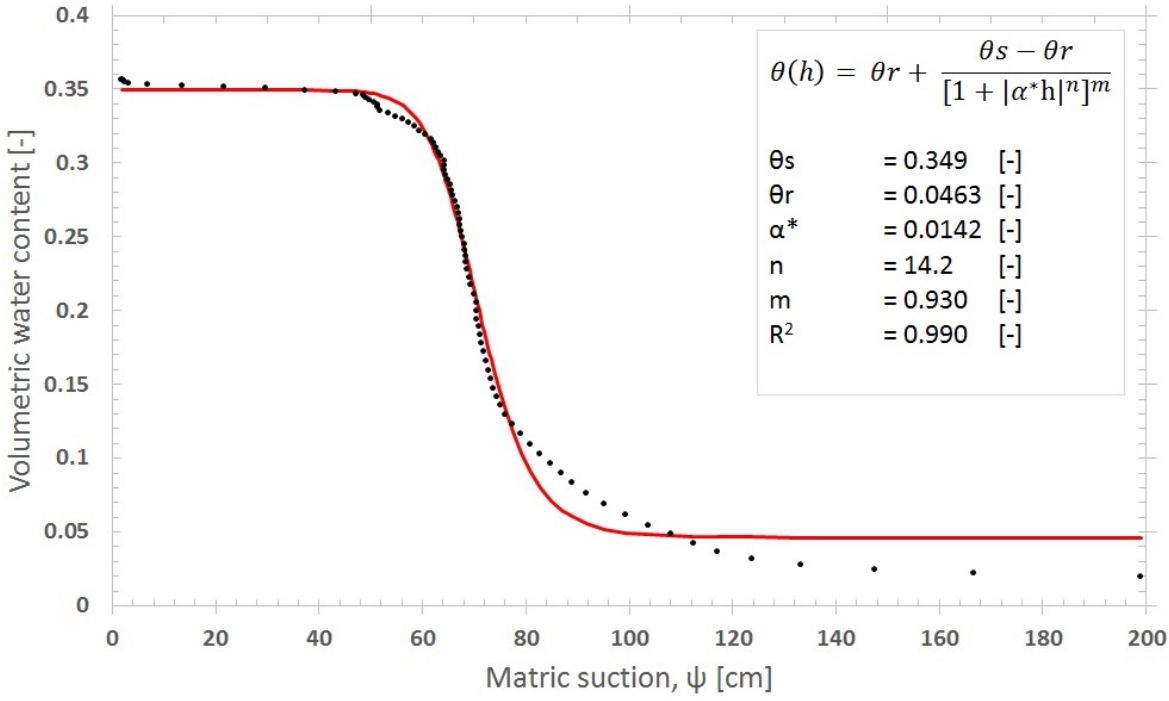

FIGURE 4.13: Retention curve of S3, fitted with the van Genuchten equation (van Genuchten, 1980).

5 Discussion

In this section, the uncertainties and arguable accuracy or precision of the methods employed in this study will be put in perspective with the results in order to specify the significance. First, main findings of the study are highlighted, after which the significance of the results are put in perspective. Secondly, any unanticipated findings are explained. Moreover, potential limitations or weaknesses in this study are identified and related to the results as a measure for validity, and finally, the results of the study will be summarized regardless of significance.

The results from this study show a clear non-monotonic behaviour of the dipersivity versus saturation relationship for coarse-grained sand. This relation provides significant information about solute transport in the vadose zone. In comparison with other studies D, it shows a better trend in dispersivity over the whole range (Maciejewski and Joswig, 2002; Maraqa et al., 1997; Padilla et al., 1999) and a higher accuracy over a larger range (Toride et al., 2003). As well, the results from this experimental work relates closely to numerical calculations done by (Raoof and Hassanizadeh, 2013). The nice relation between the In addition, this study attempts to relate the dispersivity-saturation relationship to the median grain size of the porous media. As a result, the conclusion of this study might have implications for the accuracy of modelling of vadose zone solute transport.

The equation that is developed to describe the change in dispersivity with saturation (Eq. 4.3), gives a general estimate for the range of saturation in which flow occurs in a porous medium ($\theta_r < \theta < \theta_s$). However, for theoretical water content below the residual saturation of a porous medium, the dispersivity is most likely not described accurately. In order to still be able to use the general dispersivity-saturation equation, we limit the equation's applicability to the residual saturation of the porous medium. For purposes where we need to know the dispersivity for saturations lower than the residual (pore-scale modelling), one should assume the dispersivity to be equal to only the first part of Equation 1.2, the effective diffusion coefficient.

During the experimental work, limitations of measuring in-situ pore-water electrical conductivity became evident. Concentration effects on the dielectric constant of the bulk soil were not incorporated in the calculation of pore-water electrical conductivity, hence, the calculation resulted in erroneous results. As a consequence, we assume that the bulk electrical conductivity is linearly related to the pore-water electrical conductivity and therefore the concentration, for a constant saturation. Combined with a calibration for each 5TE sensor, the bulk electrical conductivity can be converted to concentration (see Eq. 3.8 and Figure A.1).

As shown in Appendix E.1, the sensors and related employed empirical calculations (Equations 3.7, 2.1) are subject to uncertainties. Although, as we are more interested in either measuring a value that is constant over time (saturation), or the change of a value over time (concentration), we assume that the influence of the (in)accuracy of sensors is minor in

comparison to the assumption that the water content is exactly equal at all depths.

Results from analyzing the breakthrough curves of the sensor in close vicinity (5TE-3) to the bottom of the column show that there is a slight increase in pore-water velocity. The dispersion coefficient is also lower for each saturation. These results led to believe that the unit-gradient condition is not valid for the bottom the part of the column. Therefore, results from this sensor are not used in concluding the research question of this study. However, these results do show a good perspective with the results from sensor 1 (z=10.5 cm) and sensor 2 (z=18 cm). Because the results from z=10.5 and z=18 cm correlate, these results will be used in assessing the dispersivity-saturation analysis for unit-gradient condition.

Mindful readers probably noticed differences between measured θ_r in the retention data and the θ values for saturated flow experiments displayed in Table 4.1. In part, this can be attributed to packing density differences between the sample for the retention curve and the experimental column. Another cause is the error margin of the 5TE sensors for calculating volumetric water content, as evident from Equation 2.1 and Figure E.1.

As mentioned in Section 4, Equation 4.3 is constructed from experimental data of one porous medium. In order to validate the relation constructed for this porous medium, more experiments must be carried out for finer and coarser sands. If a correlation can be found between for example average grain size diameter and unsaturated dispersivity - as has been shown for the saturated dispersivity (see 4, the equation can be adapted to incorporate a change in grain size diameter. This way, the change unsaturated dispersivity is accounted for by the average grain size diameter. However, it should be noted that the heterogeneity of the sand (i.e. the variance of the particle size distribution) has a very high influence on the saturated dispersivity (Huang et al., 1995). As well, the relative change of dispersivity from saturated to unsaturated condition for a heterogeneous sand is much less (Raoof and Hassanizadeh, 2013). Therefore, it would be interesting to see what the effect of particle size variation as well as magnitude of D_{50} is on the dispersivity-saturation relationship.

6 Conclusion

This study proposed to formulate a function of dispersivity under varying saturation of multiple porous media. In pursuit of this, solute displacement has been monitored throughout an experimental column at various depths. The concentration measurements as a function of time, analytically processed using modelling software (CXTFIT, (Toride et al., 1995), provide the dispersion coefficient as a function of saturation. As a result, a relation between dispersivity and soil saturation has been established. Data in this study shows a coherence with some previous studies (Toride et al., 2003; Raoof and Hassanizadeh, 2013), while disagreeing with others (Kanzari et al., 2015; Sato, 2003; Maciejewski, 1993). The increase of α with decreasing S_w down to a saturation of about 0.50 seems to be recorded in every study. However, for lower saturations it confirms the presumption that dispersivity decreases after a certain saturation.

Results from the Advection Dispersion model show that porous medium S1 has a saturated dispersivity value of 0.05 cm. In comparison with the similary homogeneous porous media S2 and S3, the saturated dispersivity increases almost directly proportional with average grain size diameter (D_{50}). Unsaturated dispersivity for S1 increases with decreasing saturation from the saturated dispersivity until the maximum value of α = 1.32 cm at a saturation of S_w = 0.43. Dispersivity increases from intermediate saturation towards α = 0.55 cm at a saturation, S_w = 0.27. Measurements at lower saturations were not possible since this saturation was already near residual saturation. It is expected that dispersivity decreases even more with de-saturation until the residual saturation, at which point diffusion will be the dominant process of displacing solutes within the porous medium. An increase of the dispersion coefficient is measured between the first two measurements depths, where the dispersion increased with an average of 15 percent over 7.5 cm. Whether this can be solely attributed to the so called scale-effect is not likely. Results from the Mobile-Immobile model are similar to the ADE model in terms of the increase of dispersivity towards an intermediate saturation. However, dispersivity decreases at a lower saturation with respect to the ADE (0.35 to 0.43). α_m is also lower than α, however this is due to the fact that the MIM model takes into account the fractionation of mobile and immobile water portions.

A function is developed to describe the variation of dispersivity with saturation for the porous medium S1 [D_{50} = 500 μm]. Further research for finer and coarser porous media (with the same variance in particle size distribution) must show if this function can be extrapolated through intrinsic porous media characteristics (e.g. D_{50}). It is hoped that this study will provide more insight in the mechanics of solute dispersion in unsaturated soils and improve estimation of dispersion in homogeneous soils.

A Calibration data

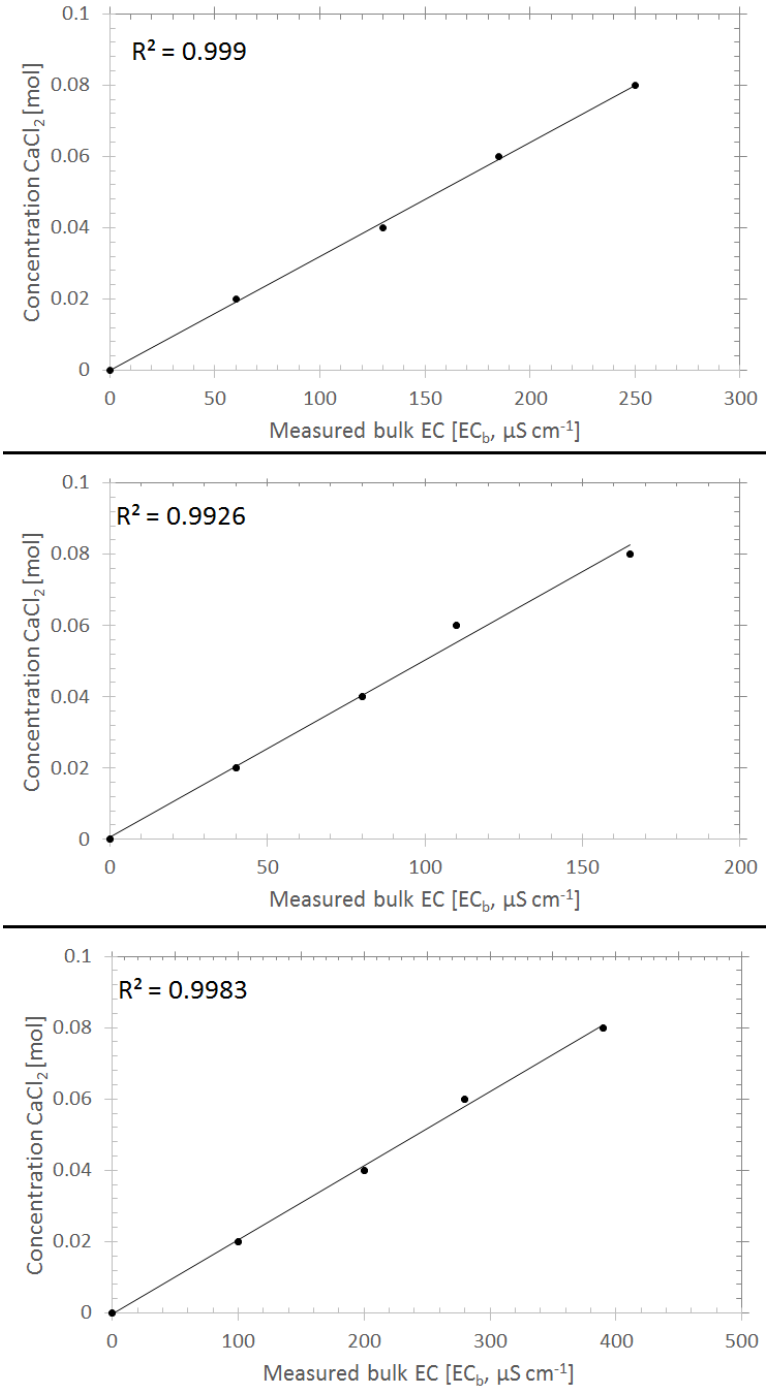

FIGURE A.1: Showing three graphs, each one representing the calibration curve for measured EC_b versus concentration. Top figure: 5TE-1, Middle figure: 5TE-2, bottom figure: 5TE-3.

B Concentration effect on permittivity

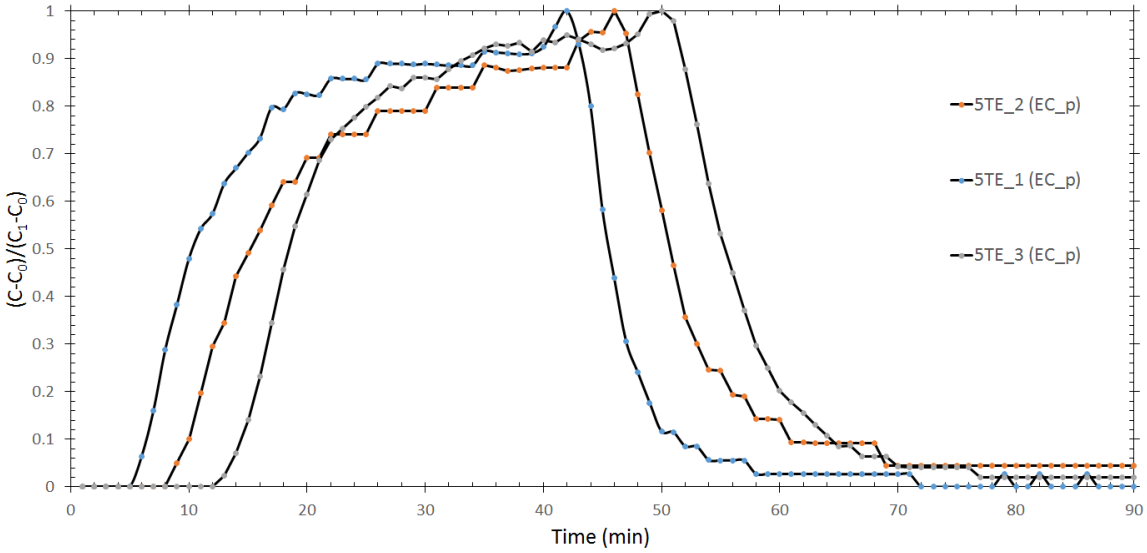

FIGURE B.1: Showing EC_p values as calculated with the equation developed by Hilhorst (Eq. 3.7)

Figure B.1 shows the normalized pore-water concentration as a result of the calculation with Equation 3.7. Here, we can see that the the data is not coherent with what we expect to happen. As can be seen from the $5TE_3$, it surpasses the concentration from $5TE_2$, which is most likely not true for a homogeneous porous medium, as we expect $5TE_2$ to reach maximum concentration before $5TE_3$. Also, the concentration spike at t = 42, 46, and 50, respectively for the first, third, and second sensor, is a result of permittivity change due concentration effect of the inserted tracer. It should be noted that this effect is lower at concentrations up to 0.02 M, however, for these concentrations we do not measure accurate breakthrough curves, since the measurement resolution is too large.

C Dispersivity-Saturation relation at three different depths

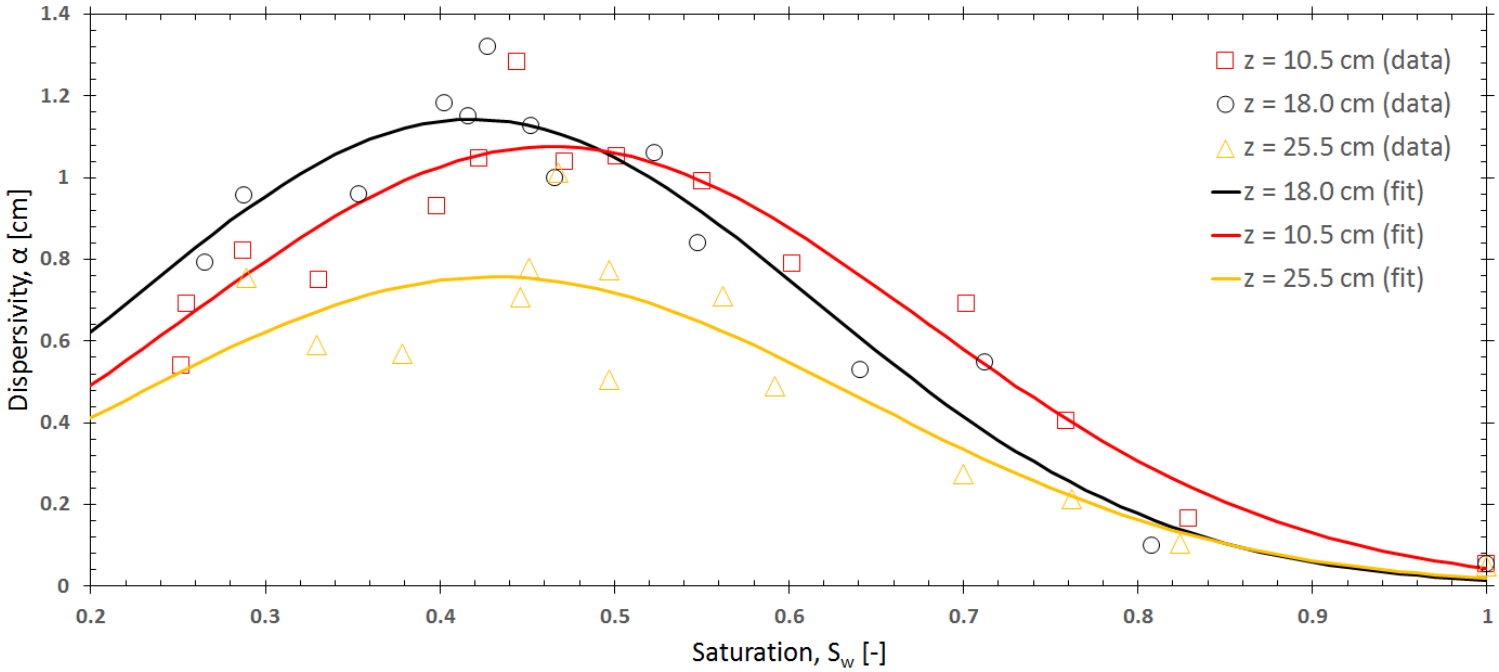

FIGURE C.1: Showing the α - S_w relation for all three depths, including a separately fitted Gaussian function

D Dispersivity-Saturation relation compared to literature

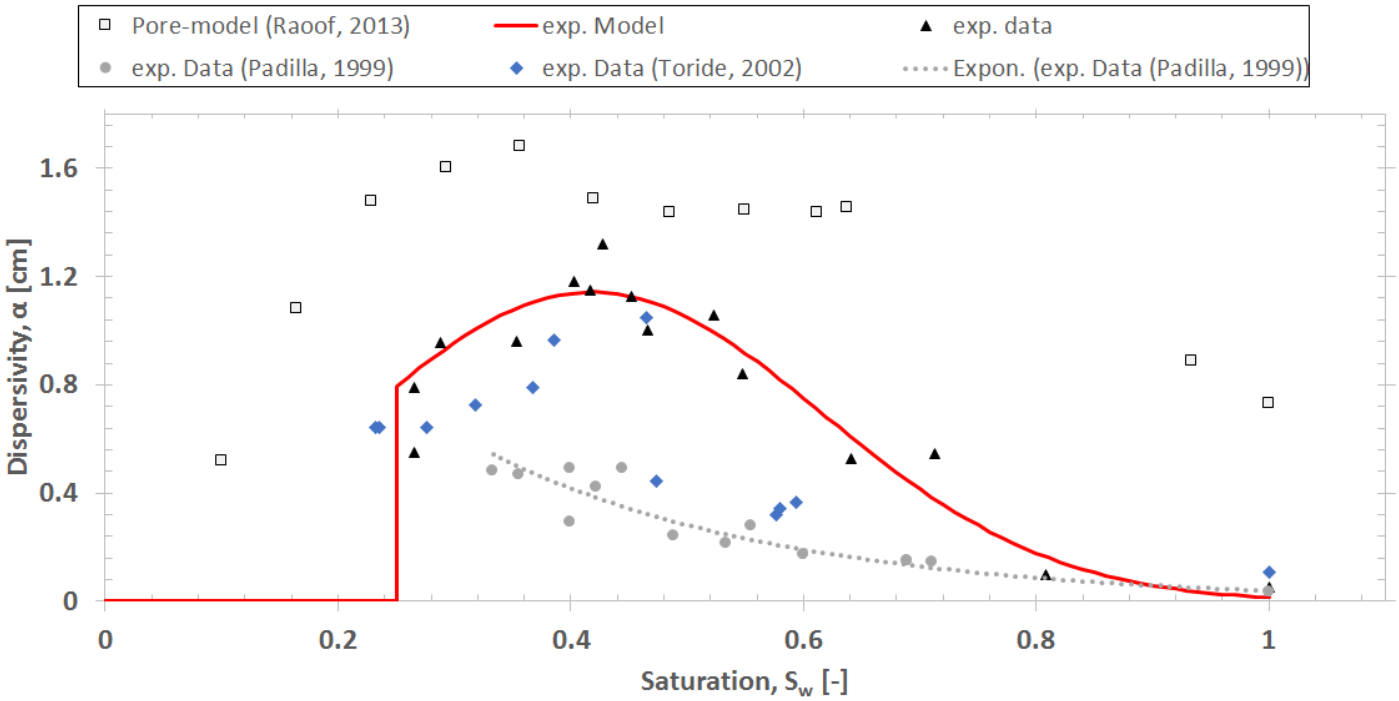

FIGURE D.1: Showing the α - S_w relation for the results from this study, the model values using Equation 4.3, the experimental results by Toride et al. (2003), Padilla et al. (1999) and pore-scale results by Raoof and Hassanizadeh (2013)

E 5TE Specifications

2.1 Specifications

Volumetric Water Content

Range: Apparent dielectric permittivity (ε_a): 1 (air) to 80 (water)

Resolution: ε_a: 0.1 ε_a (unitless) from 1 to 20, < 0.75 ε_a (unitless) from 20 to 80 VWC: 0.0008 m^3/m^3(0.08% VWC) from 0 to 50% VWC

Accuracy: ε_a: ± 1 ε_a (unitless) from 1 to 40 (soil range), $\pm 15\%$ from 40 to 80 (VWC)

- Using Topp equation: ± 0.03 m^3/m^3($\pm 3\%$ VWC) typical in mineral soils that have solution electrical conductivity < 10 dS/m
- Using medium specific calibration, ± 0.01 to 0.02 m^3/m^3(± 1 to 2% VWC) in any porous medium.

Electrical Conductivity (bulk)

Range: 0 to 23 dS/m (bulk)

Resolution: 0.01 dS/m from 0 to 7 dS/m, 0.05 dS/m from 7 to 23 dS/m

Accuracy: $\pm 10\%$ from 0 to 7 dS/m, user calibration required above 7 dS/m.

FIGURE E.1: Shows specifications of the 5TE sensor used for measuring permittivity, electrical conductivity and temperature, from Decagon Devices (2016)

Bibliography

Bear, J. (1972). Dynamics of Fluids in Porous Media. *Soil Science*, 120(2):162–163.

De Smedt, F. and Wierenga, P. J. (1984). Solute Transfer Through Columns of Glass Beads. *Water Resources Research*, 20(2):225–232.

Decagon Devices, I. (2016). 5TE Manual.

Fitts, C. R. (2002). *Groundwater Science*. Academic Press.

Folk, R. L. (1966). A REVIEW OF GRAIN-SIZE PARAMETERS.

Freeze, R. and Cherry, J. (1979). *Groundwater*. Prentice-Hall, Englewood Cliffs, N.J.

Gelhar, L. W., Welty, C., and Rehfeldt, K. R. (1992). A critical review of data on field-scale dispersion in aquifers.

Gupta, R., Millington, R., and Klute, A. (1973). Hydrodynamic dispersion in unsaturated porous media. I. Concentration distribution during dispersion. *J. Indian Soc. Soil Sci.*, (21):1–7.

Hilhorst, M. (2000). A Pore Water Conductivity Sensor. *Soil Science Society of America Journal*, 64(6):1922–1925.

Huang, K., Toride, N., and van Genuchten, M. T. (1995). Experimental Investigation of Solute Transport in Large, Homogeneous and Heterogeneous, Saturated Soil Columns. *Transp. Porous Media*, 18(1):283–302.

Kanzari, S., Hachicha, M., and Bouhlila, R. (2015). Laboratory Method for Estimating Solute Transport Parameters of Unsaturated Soils Laboratory Method for Estimating Solute Transport Parameters of Unsaturated Soils. 1:149–154.

Khan, A. U. H. and Jury, W. A. (1990). A laboratory study of the dispersion scale effect in column outflow experiments. *Journal of Contaminant Hydrology*, 5(2):119–131.

Krupp, H. and Elrick, D. (1968). Miscible displacement in an unsaturated glass bead media. *Water Resources Research*, (4):809–815.

Lewis, J. and Sjostrom, J. (2010). Optimizing the experimental design of soil columns in saturated and unsaturated transport experiments. *Journal of Contaminant Hydrology*, 115(1-4):1–13.

Maciejewski, S. (1993). Numerical and experimental study of solute transport in unsaturated soils. *Journal of contaminant hydrology*, 14:193–206.

Maciejewski, S. and Joswig, K. (2002). Estimation of water saturation dependence of dispersion in unsaturated porous media : experiments and modelling analysis. *Advances in Water Resources*, 25:565–576.

Maraqa, M. A., Wallace, R. B., and Voice, T. C. (1997). Effects of degree of water saturation on dispersivity and immobile water in sandy soil columns. *Journal of Contaminant Hydrology*, 25(3-4):199–218.

Millington, R. J. and Quirk, J. P. (1961). Permeability of porous solids. *Transactions of the Faraday Society*, 57(0):1200–1207.

Nützmann, G., Thiele, M., Maciejewski, S., and Joswig, K. (1998). Inverse modelling techniques for determining hydraulic properties of coarse-textured porous media by transient outflow methods. *Advances in Water Resources*, 22(3):273–284.

Oliviera, I. B., Demond, A. H., and Salehzadeh, A. (1996). Packing of Sands for the Production of Homogeneous Porous Media. *Soil Sci. Soc. Am. J.*, 60(1):49–53.

Padilla, I. Y., Yeh, T. C. J., and Conklin, M. H. (1999). The effect of water content on solute transport in unsaturated porous media. *Water Resources Research*, 35(11):3303–3313.

Raoof, A. and Hassanizadeh, S. M. (2013). Saturation-dependent solute dispersivity in porous media: Pore-scale processes. *Water Resources Research*, 49(4):1943–1951.

Sato, T. (2003). Solute dispersion in a variably saturated sand. *Water Resources Research*, 39(6):1–7.

Schindler, U., Durner, W., von Unold, G., Mueller, L., and Wieland, R. (2010). The evaporation method: Extending the measurement range of soil hydraulic properties using the air-entry pressure of the ceramic cup. *Journal of Plant Nutrition and Soil Science*, 173(4):563–572.

Topp, G. C., Davis, J. L., and Annan, A. P. (1980). Electromagnetic Determination of Soil Water Content:. *Water Resources Research*, 16(3):574–582.

Toride, N., Inoue, M., and Leij, F. J. (2003). Hydrodynamic dispersion in an unsaturated dune sand. *Soil Science Society of America Journal*, 67(3):703–712.

Toride, N., Leij, F. J., and van Genuchten, M. (1995). The CXTFIT Code for Estimating Transport Parameters from Laboratory or Field Tracer Experiments. Version 2.0. Research Report No. 137. U. S. Department of agriculture, Riverside (CA).

van Genuchten, M. T. (1980). A Closed-form Equation for Predicting the Hydraulic Conductivity of Unsaturated Soils1.

van Genuchten, M. T., Leij, F. J., and Yates, S. R. (1991). The RETC Code for Quantifying the Hydraulic Functions of Unsaturated Soils. *United States Environmental Reseach Laboratory*, (December):93.